

SEISMIC DISPLACEMENT DEMANDS ON SELF-CENTERING
SINGLE-DEGREE-OF-FREEDOM SYSTEMS

Changxuan Zhang
M.A.Sc. Thesis

McMaster University
Dept. of Civil Engineering

SEISMIC DISPLACEMENT DEMANDS ON SELF-CENTERING
SINGLE-DEGREE-OF-FREEDOM SYSTEMS

By:
CHANGXUAN ZHANG
B.ENG. (Central South University)

A Thesis Submitted to the School of Graduate Studies in Partial Fulfilment of the
Requirements for the Degree of Master of Applied Science

McMaster University
© Copyright by Changxuan Zhang, September 2015

Changxuan Zhang
M.A.Sc. Thesis

McMaster University
Dept. of Civil Engineering

MASTER OF APPLIED SCIENCE (2015)
(CIVIL ENGINEERING)

McMaster University
Hamilton, Ontario, Canada

Title: Seismic Displacement Demands of Self-Centering Single-Degree-of-Freedom Systems
Author: Changxuan Zhang, B.Eng. (Central South University)
Advisor: Lydell Wiebe
Number of Pages: xiii, 69

ABSTRACT

Most conventional seismic design intends for key structural members to yield in order to limit seismic forces, leading to structural damage after a major earthquake. To minimize this structural damage, self-centering systems are being developed. But how to estimate the peak seismic displacement of a self-centering system remains a problem for practical design. This thesis addresses this need by presenting a parametric study on the seismic displacement demands of single-degree-of-freedom (SDOF) systems with flag-shaped hysteresis considering 13,440,000 nonlinear time history analyses. Ground motion records that represent seismic hazards in active seismic regions with stiff soil and rock site conditions are used. The influences of the four independent parameters that define a flag-shaped hysteresis are presented in terms of median displacement ratios, facilitating the design-level estimation of nonlinear displacement demands on self-centering systems from the spectra displacements of elastic systems. The influence of initial period on self-centering systems is similar to its influence on traditional systems with elastoplastic hysteresis, but a much lower linear limit can be adopted for self-centering systems while achieving acceptable peak displacements. Supplemental energy dissipation suppresses the peak displacement but additional energy dissipation becomes less effective as more is added. The effect of nonlinear stiffness is small as long as it is positive and close to zero, but a negative nonlinear stiffness can lead to unstable response. Self-centering systems located on rock sites usually have smaller displacement demands than those on stiff soil sites. When the damping ratio is increased or decreased, the displacement ratios do not necessarily decrease or increase consistently. A tangent stiffness proportional damping model is considered, leading to a significant increase in displacement demands but similar overall trends. Based on the observations, regression analysis is used to develop a simplified equation that approximates the median inelastic displacement ratios of self-centering systems for design.

ACKNOWLEDGEMENT

The encouragement, support and contribution of many people have made this thesis possible. Space allows me to name only a few.

First, I would like to thank my supervisor, Lydell Wiebe, for his guidance, patience and encouragement throughout my education at McMaster. He is the supervisor who not only gave me necessary input but also helped me himself when I got stuck. His encouragement also goes beyond the academic work to let me explore and enjoy my life in Canada. I am deeply inspired by his willingness to help and great supervision.

I am also thankful for my teachers at McMaster University, Dr. Dimitrios Konstantinidis, Dr. Wael El-Dakhakhni, Dr. Michael Tait and Dr. Tracy Becker. All the courses laid a solid foundation for me in earthquake engineering and really facilitated my research.

I would give many thanks to all my colleagues and friends at McMaster. Including but not limited to Niel Van Engelen, Mohamed Ezzeldin, Taylor Steele, Saman Rastgoo Moghadam, Ahmad Siam: thank you for your help throughout my years of study and research. The education experience together with you guys will be a life long treasure for me. Particular thanks are given to Kuan Lin, who gave me access to the great computational power without which I can not finish the huge amount of analyses.

I would like to acknowledge the financial support from the Department of Civil Engineering, McMaster University, without which I would have been a starving student.

I am particularly grateful to my dad and mom back home in China for their unceasing support and encouragement during my studies.

TABLE OF CONTENTS

CHAPTER 1: INTRODUCTION	1
1.1 Overview of Self-centering Systems.....	1
1.2 Seismic Displacements of Self-Centering SDOF Systems.....	7
1.2.1 Summary of Previous Studies.....	7
1.2.2 Limitations of Previous Studies.....	10
1.3 Research Objectives.....	11
CHAPTER 2: DEFINITION OF PARAMETERS AND EXAMPLE ANALYSES .	13
2.1 Hysteretic Parameters.....	13
2.1.1 Initial Period.....	13
2.1.2 Tangent Period.....	15
2.1.3 Force Reduction Factor.....	16
2.1.4 Hysteretic Energy Dissipation Parameter.....	17
2.2 Inherent Damping Model.....	18
2.2.1 Initial Stiffness Proportional Damping Model.....	18
2.2.2 Tangent Stiffness Proportional Damping Model.....	19
2.3 Ground Motion Records.....	20
2.4 Numerical Solution Technique.....	22
2.5 Analysis Example.....	23
CHAPTER 3: RESULTS OF PARAMETRIC STUDY	27
3.1 Initial Damping Model.....	27
3.1.1 Baseline Study.....	27
3.1.2 2% and 10% initial damping.....	36
3.1.3 Ground Motions Recorded on Rock Sites.....	39
3.2 Tangent Damping Model.....	41
3.2.1 Problem with Initial Damping Model.....	41
3.2.2 Influence of Different Hysteretic Parameters.....	43
3.3 84th Percentile Displacement Demands.....	49

CHAPTER 4: REGRESSION ANALYSIS	53
4.1 Previous Proposals	53
4.2 Form of Regression Equation.....	55
4.3 Calibration of Regression Equation	57
4.4 Evaluation of Regression	59
CHAPTER 5: CONCLUSIONS AND RECOMMENDATIONS	62
5.1 Conclusions.....	62
5.2 Recommendations for Future Work.....	64
REFERENCES	66

APPENDIX A: VALIDATION OF NUMERICAL SOLUTION TECHNIQUE

APPENDIX B: REGRESSION FOR MEAN VALUE

LIST OF FIGURES

Figure 1.1 Push-pull response of a self-centering system	3
Figure 1.2 Different types of self-centering systems	4
Figure 1.3 Flag-shaped Hysteresis	5
Figure 1.4 Design procedure for a controlled rocking steel braced frame (after Wiebe and Christopoulos 2014)	6
Figure 2.1 Flag-shaped hysteresis	13
Figure 2.2 Definition of force reduction factor	17
Figure 2.3 Ground motion records: a) acceleration spectra; b) displacement spectra.....	21
Figure 2.4 Example Analyses: a) time history; b) hysteresis	24
Figure 2.5 Example Analyses: a) individual and median displacement; b) individual and median displacement coefficient.....	25
Figure 3.1 Displacement Ratios of Self-Centering SDOF Systems with Respect to Initial Period with Initial Damping Model and $T_{\tan} = \infty$	28
Figure 3.2 Displacement Ratios of Self-Centering SDOF Systems with Respect to Force Reduction Factor with Initial Damping Model	29
Figure 3.3 Effect of Extremely Large Force Reduction Factor: a) Hysteresis Shape; b) Time History Response.....	31
Figure 3.4 Displacement Ratios of Self-Centering SDOF system with Respect to Hysteretic Energy Dissipation Parameter with Initial Damping Model	32
Figure 3.5 Displacement Ratios of Self-Centering SDOF System with Respect to Tangent Period with Initial Damping Model	34
Figure 3.6 Collapse Mechanism	36
Figure 3.7 Relative Difference of Displacement Ratios between 2% and 5% Damping Ratio.....	37

Figure 3.8 Relative Difference of Displacement Ratios between 5% and 10 Damping Ratio	38
Figure 3.9 Comparison of Displacement Ratios on Rock Sites and Stiff Soil Sites	40
Figure 3.10 Comparison of Structural Force and Damping Force for $T_0 = 0.5s$, $\beta = 0.5$ and $T_{tan} = \infty$	42
Figure 3.11 Displacement Ratios of Self-Centering SDOF System with Respect to Initial Period with Tangent Damping Model and $T_{tan} = \infty$	44
Figure 3.12 Displacement Ratios of Self-Centering SDOF System with Respect to Force Reduction Factor with Tangent Damping Model.....	45
Figure 3.13 Displacement Ratios of Self-Centering SDOF Systems with Respect to Hysteretic Energy Dissipation Parameter with Tangent Damping Model.....	47
Figure 3.14 Displacement Ratios of Self-Centering SDOF Systems with Respect to Tangent Period with Tangent Damping Model.....	48
Figure 3.15 84th Percentile Displacement Ratios with $T_{tan} = \infty$	50
Figure 3.16 84th Displacement Ratios with $T_0 = 0.5s$	51
Figure 4.1 Residuals for Seo's Equation for Large R (based on Seo 2005)	54
Figure 4.2 Relative Error between Predicted and Observed Displacement Demands (with $T_{tan} = \infty$).....	60
Figure 4.3 Relative Error between Predicted and Observed Displacement Demands with Tangent Period of $10s$	61

LIST OF TABLES

Table 2.1 Parameters Considered	14
Table 4.1 Parameters Considered in Regression Analysis	58
Table 4.2 Coefficient from Regression Analyses	59
Table A.1 Displacement ductility with $\alpha = 0.02$	A-4
Table A.2 Displacement ductility with $\alpha = 0.10$	A-5
Table A.3 Displacement ductility with $\alpha = 0.20$	A-6
Table A.4 Displacement ductility with $\alpha = 0.35$	A-7
Table A.5 Summary of results checking with $T_0 = 0.2s$ and $R = 2$	A-9
Table A.6 Summary of results check with $T_0 = 1.0s$ and $R = 2$	A-10
Table A.7 Summary of results check with $T_0 = 2.0s$ and $R = 2$	A-11
Table B.1 Coefficients from regression analyses (Mean)	B-1

LIST OF ABBREVIATIONS AND SYMBOLS

α	stiffness ratio of a self-centering system
β	hysteretic energy dissipation parameter of flag-shaped hysteresis or Newmark's constant in numerical solution technique
$b_i(1 \leq i \leq 5)$	constants to be determined by regression
$c_i(1 \leq i \leq 6)$	constants to be determined by regression
c	damping coefficient
c_i	initial stiffness proportional damping model or damping coefficient at current time step
c_t	tangent stiffness proportional damping model
C_R	(median or 84 th percentile) displacement ratio
$C_{R,5\%}$	median displacement ratio with initial stiffness proportional damping model when $\zeta = 5\%$
$C_{R,2\%}$	median displacement ratio with initial stiffness proportional damping model when $\zeta = 2\%$
$C_{R,10\%}$	median displacement ratio with initial stiffness proportional damping model when $\zeta = 10\%$
$C_{R,rock}$	median displacement ratio using ground motion records from rock sites
$C_{R,soil}$	median displacement ratio using ground motion records from stiff soil sites
C_V	seismic zone and site class type factor
$\Delta_{elastic}$	peak displacement of an elastic system when subjected to an earthquake
$\Delta_{nonlinear}$	peak displacement of a self-centering system when subjected to an earthquake
η	strength ratio
$f_{elastic}$	peak force in an elastic system when subjected to an earthquake
f_y	linear limit of a flag-shaped hysteresis
FEMA	Federal Emergency Management Agency
γ	Newmark's constant in numerical solution technique
I	importance factor
m	mass of a system (assumed unity)
M	magnitude of an earthquake
$M_{b,rock}$	base rocking moment of a controlled rocking steel braced frames

M_w	moment resisting capacity of a controlled rocking steel braced frame
$\bar{\mu}_\Delta$	displacement ductility
k_0	initial stiffness of an elastic system or a self-centering system
k_{i-1}	stiffness of a nonlinear system at previous time step
PEER	Pacific Earthquake Engineering Research Center
R	force reduction factor
Residual	the difference between predicted displacement ratio and observed displacement ratio normalized by the observed displacement ratio
SDOF	single-degree-of-freedom
T_0	initial period of a self-centering system or natural period of an elastic system
T_{\tan}	tangent period of a self-centering system
V_y	base shear
W	weight of the structure
ζ	damping ratio

DECLARATION OF ACADEMIC ACHIEVEMENT

The research and analysis work presented in this thesis was carried out solely by Changxuan Zhang (author) with advice and guidance from the academic supervisor Dr. Lydell Wiebe. Information presented from outside sources has been cited when appropriate. All other materials are the sole work of the author.

CHAPTER 1:

INTRODUCTION

1.1 Overview of Self-centering Systems

Most modern seismic design is based on intentionally designing an inelastic deformation mechanism that involves yielding at certain locations. Members at those locations are designed to exhibit a stable hysteretic response that limits seismic forces and dissipates energy, while other parts of the structure are designed to remain elastic. This process is termed capacity design (Park and Paulay 1975). The objective is that structural collapse is prevented and people can be evacuated safely after a major earthquake event. This design philosophy has proved to meet these objectives in recent earthquake events (Kam et al. 2010, Clifton et al. 2011). Nevertheless, even though most structures did not collapse during the earthquakes, large inelastic deformations occurred that are associated with structural damage and residual displacements. The structural damage needs repair afterwards and the residual displacements also have a strong influence on the possibility and cost of repair (Iwata et al. 2005, McCormick et al. 2008).

To avoid these structural damage and residual deformations, the concept of self-centering systems is drawing increasing attention (Kurama 2000, Wiebe and Christopoulos 2014). A self-centering system also has a nonlinear mechanism

that limits seismic forces for capacity design, but after a major earthquake, a self-centering structure returns to an essentially undeformed position without any residual displacements.

One type of self-centering system is a controlled rocking wall, which is shown schematically in Fig. 1.1. For this discussion, it is assumed that the wall-foundation interface has no flexibility and the energy dissipation devices are rigid-perfectly plastic. When there is no lateral force, the wall stands on the foundation with the reaction forces uniformly distributed along the surface as shown in Fig.1.1(a). As lateral load is applied and increased, the reaction force distribution changes until a critical point is reached when the reaction force at one corner becomes zero (Fig.1.1(b)). As the lateral load keeps increasing, the energy dissipation devices are activated to take load and the forces in the devices increase until yield (Fig.1.1(c)). If the energy dissipation devices are perfectly rigid before yielding, the gap will remain closed until the energy dissipation devices yield (point c in the force-displacement relationship). After the energy dissipation devices yield, the gap-opening mechanism initiates and the system enters its nonlinear stiffness range, where the stiffness is provided by the post-tensioning elongation (Fig.1.1(d)). When the lateral load is removed and the wall is loaded in the opposite direction, the energy dissipation devices yield in compression, the gap closes and a similar response is seen on the other direction (Fig.1.1(e)). When the lateral load is removed, the post-tensioning and the wall's self-weight return the wall to its original position without any structural

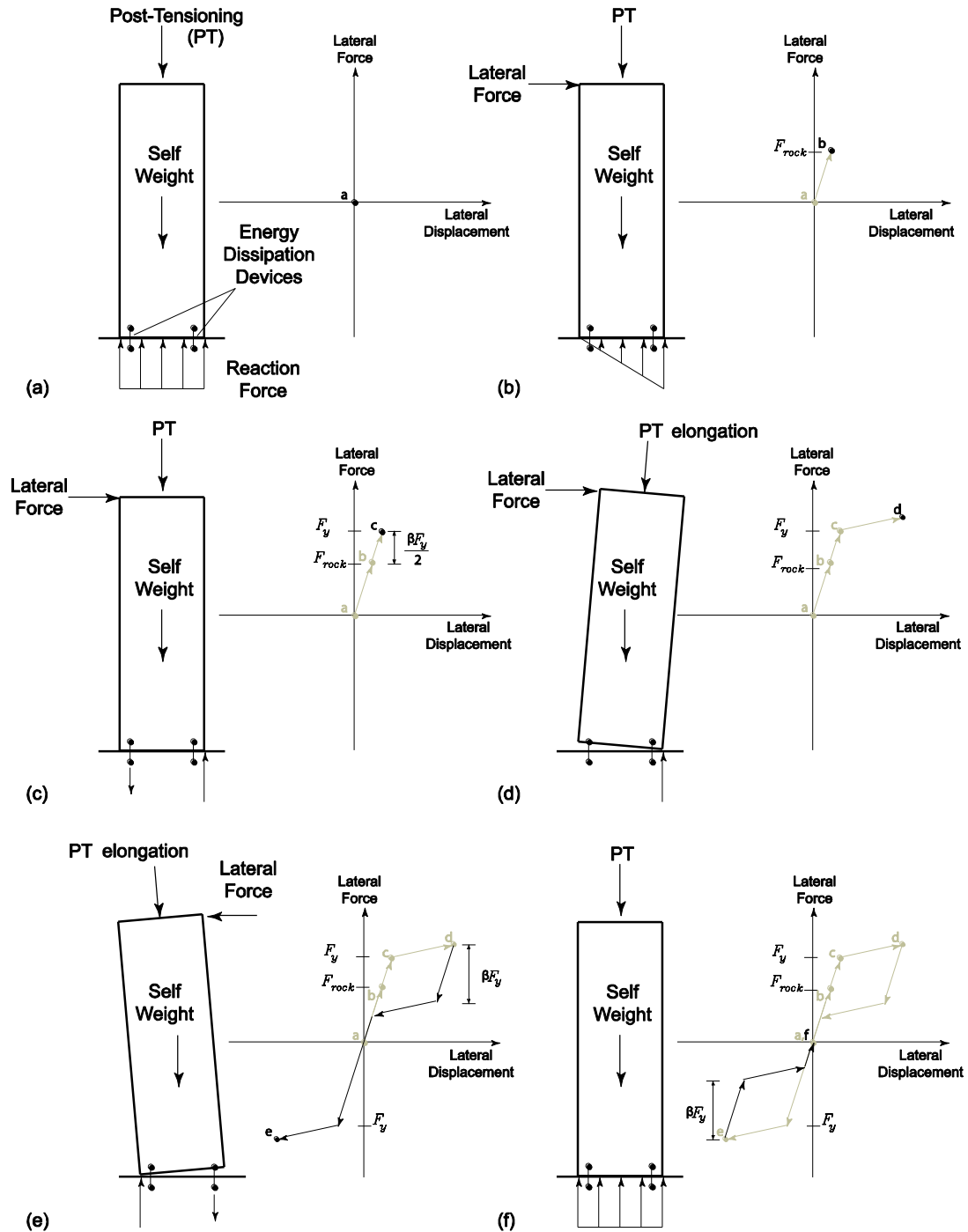


Figure 1.1 Push-pull response of a self-centering system: (a) at rest; (b) activation of energy dissipation devices; (c) yielding of damping device; (d) gap opening mechanism initiation; (e) reverse direction nonlinear mechanism; (f) returning to original position when load removed

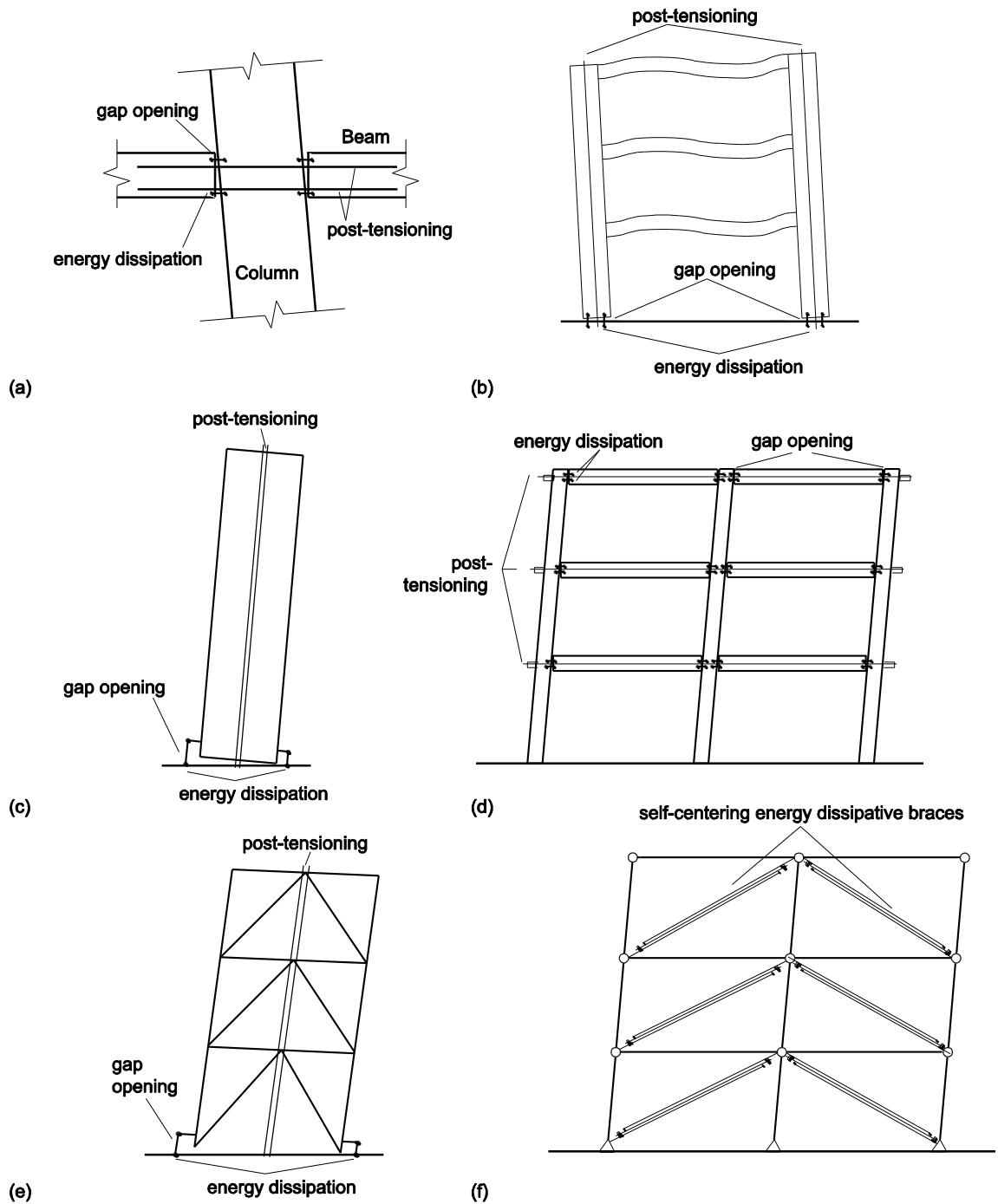


Figure 1.2 Different types of self-centering systems: (a) reinforced concrete rocking joint; (b) unbonded post-tensioning precast concrete rocking frame; (c) unbonded post-tensioned precast concrete rocking wall; (d) post-tensioned steel moment frame; (e) controlled rocking steel braced frame; (f) steel braced frame with self-centering energy dissipative braces

damage or residual displacement.

A similar self-centering mechanism can be applied to reinforced concrete frame rocking joints (e.g. Priestley and Tao 1993) (Fig.1.2(a)), unbonded post-tensioned precast concrete rocking frames (e.g. Roh and Reinhorn 2010) (Fig.1.2(b)) and walls (e.g. Kurama 2000) (Fig.1.2(c)), steel moment frame connections (e.g. Christopoulos et al. 2002) (Fig.1.2(d)), controlled rocking steel braced frames (e.g. Ma et al. 2011, Wiebe 2013) (Fig.1.2(e)) and self-centering energy dissipative braces (Erochko et al. 2013) (Fig.1.2(f)).

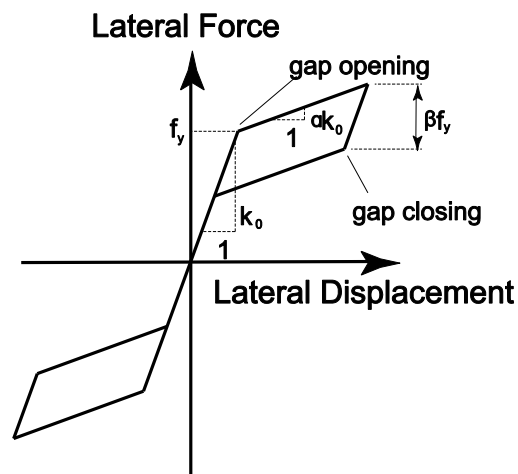


Figure 1.3 Flag-shaped Hysteresis

While the aforementioned self-centering systems have different mechanisms, their force-displacement relationships can all be idealized as a flag-shaped hysteresis (Fig. 1.3). The designer must select the target hysteretic properties

(initial stiffness k_0 , linear limit f_y , energy dissipation parameter β , nonlinear stiffness αk_0) in order to design the self-centering mechanism.

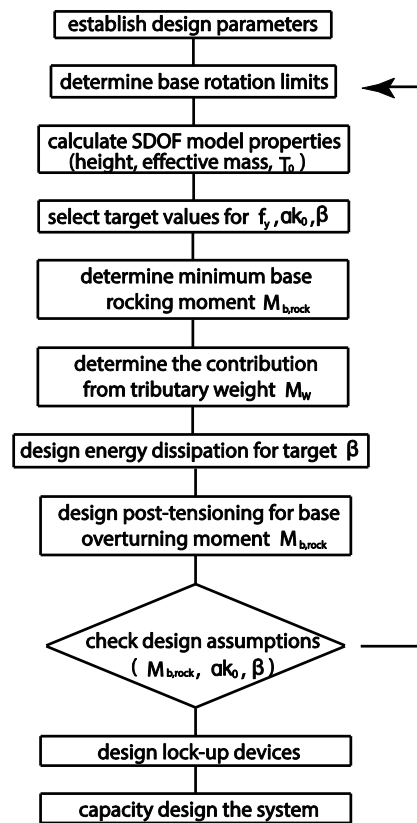


Figure 1.4 Design procedure for a controlled rocking steel braced frame (after Wiebe and Christopoulos 2014)

For example, a proposed design procedure for self-centering steel braced frames (Fig.1.2(e)) is shown in Fig. 1.4 (Wiebe and Christopoulos 2014). This design process assumes that the peak displacement of a self-centering structure can be

estimated from a self-centering single-degree-of-freedom (SDOF) system. Based on this assumption, the energy dissipation and post-tensioning are designed to achieve target hysteretic parameters (k_0, f_y, β and αk_0 in Fig.1.3), that will meet the selected base rotation (i.e. displacement) limits. Thus, there is a need to determine how these hysteretic parameters affect the displacement demands of self-centering SDOF systems. Similarly, in conventional force-based design, the displacement must be checked against codified limits. This also requires an ability to predict the displacement response of self-centering systems. So it is important to study seismic responses of SDOF systems with flag-shaped hysteresis.

1.2 Seismic Displacements of Self-Centering SDOF Systems

1.2.1 Summary of Previous Studies

Christopoulos et. al. (2002) studied the displacement demands of self-centering SDOF systems in terms of ductility demands. A strength ratio was used in that study with different combinations of $\alpha = 0.02, 0.10, 0.20, 0.35$ and $\beta = 0, 0.3, 0.6, 1.0$. The strength ratio, η , was defined as the ratio of the design base shear and the seismic weight and the value of $5\% \leq \eta \leq 100\%$ was considered. For the ground motions considered, the range of strength ratios in this study corresponds to a force reduction factor R (see Section 2.1.3) in the range of 4.5-8.5. Considering an initial stiffness proportional damping model (see Section 2.2.1), it was concluded that self-centering systems can achieve similar or reduced ductility

demands compared to traditional systems with elastoplastic hysteresis. It was also concluded that less absorbed energy for self-centering systems than for traditional elastoplastic systems is not a problem because the importance of this response index is minimal as cumulative damage is limited to replaceable energy dissipation devices. The ground motion records used in this study were from relatively stiff soil sites.

Seo and Sause (2005) also studied self-centering SDOF systems in terms of displacement ductility. They considered a force reduction factor R of 2–6 and a similar range of α and β as Christopoulos et al. (2002). They compared the response of self-centering SDOF systems to that of traditional SDOF systems represented by elastoplastic and stiffness degrading hysteresees. It was found that self-centering systems have much higher ductility demands compared to elastoplastic and stiffness degrading systems when using the same force reduction factor R and nonlinear stiffness ratio α , particularly when β is small, but can achieve similar ductility demands by combining different α and β . Both an initial frequency proportional damping model and a secant frequency proportional damping were considered in this study, the latter of which means that the damping is changed according to the secant frequency of the SDOF system as the system enters the nonlinear range. The secant damping model did not affect the trends of ductility demands significantly but did increase the ductility demands (by as much as 200%) and affect the effectiveness of hysteretic

parameters in reducing the ductility demands. The secant frequency proportional damping model will be called the secant stiffness proportional damping model in the following context as frequency is related to stiffness. The authors also considered the effect of site soil conditions and found that ductility demands for self-centering systems with low strength ($R = 6$) on rock sites and soft rock sites are lower than those on stiff soil sites, especially at short initial periods ($T_0 < 1.25s$), where the ductility demands of self-centering SDOF systems on rock sites can be as little as 50% of the ductility demands of self-centering SDOF systems on stiff soil sites. Seo (2005) proposed an equation in the following form to predict the displacement demand on self-centering SDOF systems:

$$C_R = R^{\exp(f(\alpha, \beta, T_0))}$$
$$f(\alpha, \beta, T_0) = \frac{(a - b\sqrt{\alpha})^2}{T_0^{(c-d\sqrt{\alpha})^2}} - 1 \quad (1-1)$$

where a , b , c , d are constants that are read from a table depending on β .

Wiebe and Christopoulos (2014) studied self-centering SDOF systems in terms of absolute peak displacement and converted the results into interstory drift using an assumed period-height relationship. Using nine different combinations of nonlinear stiffness and β , they developed charts for design usage assuming an initial stiffness proportional damping model. An initial period range of 0.2–2.0s was used, and they concluded that the peak interstory drifts generally increase with decreasing initial period and increasing force reduction factor. They also

found that the design approach to estimate peak displacements should be based on the initial stiffness rather than the secant stiffness because the results were much more sensitive to the initial period than to the stiffness in the nonlinear range. Additionally, it was found that the energy dissipation parameter is most effective to reduce displacements around $R=10$ and that the nonlinear stiffness has little influence on peak displacements.

1.2.2 Limitations of Previous Studies

In the first two studies above (Christopoulos et al. 2002, Seo and Sause 2005), the self-centering systems were defined with linear limits (f_y in Fig.1.3) that are similar to the strength of traditional elastoplastic systems. However, Wiebe and Christopoulos (2014) suggested that a larger value of R (reduced f_y in Fig.1.3) can be used for self-centering systems than traditional systems while still limiting the drift to the code specified value of 2.5% (NRCC 2010) during a maximum considered earthquake.

Also, none of the previous studies has considered the effect of a negative nonlinear stiffness caused by significant $P-\Delta$ effect. Research on traditional systems has showed that a negative nonlinear stiffness can lead to collapse (FEMA P440A). Thus, it is worthwhile to explore the influence of negative nonlinear stiffness on self-centering SDOF systems.

Additionally, Christopoulos et al. (2002) and Wiebe and Christopoulos (2014) used only an initial stiffness proportional damping model in their studies. Seo and Sause (2005) considered both an initial stiffness proportional damping model and a secant stiffness damping model. However, some recent studies stated that a tangent stiffness proportional damping model is a more realistic assumption for inelastic systems (Leger and Dussault 1992, Priestley and Grant 2005, Charney 2008). Therefore, it is necessary to consider a tangent stiffness proportional damping model and compare the difference between the initial stiffness proportional damping model and the tangent stiffness proportional damping model for self-centering SDOF systems.

Last but not least, Christopoulos et al. (2002) and Wiebe and Christopoulos (2014) showed the general trend of ductility demands and displacement demands respectively, but did not quantify the trend with an equation. The equation proposed by Seo (2005) is based on results of $R = 2 - 8$ with an accuracy of 25% for the values included in the regression and may not be valid beyond this range. Furthermore, a simpler equation is desired for practical application.

1.3 Research Objectives

Based on the research limitations noted above, the main purpose of this study is to extend the previous studies on self-centering SDOF systems (Christopoulos et

al. 2002, Seo and Sause 2005, Wiebe and Christopoulos 2014) to consider and quantify the influence of:

1. large force reduction factors;
2. negative nonlinear stiffness;
3. the tangent stiffness proportional damping model;
4. difference between rock site conditions and stiff soil site conditions.

Chapter 2 summarizes how the hysteretic parameters are normalized, describes the numerical solution technique and gives an example of the analyses. The analyses results are presented in Chapter 3 with detailed discussions.

The end objective of this work is to develop an equation that predicts the peak displacements of self-centering SDOF systems and that is simple enough for routine design. Such an equation is developed in Chapter 4 using nonlinear regression analysis, and accuracy of the developed equation is also evaluated there.

Chapter 5 summarizes the work and future research needs.

CHAPTER 2:

DEFINITION OF PARAMETERS AND EXAMPLE ANALYSES

2.1 Hysteretic Parameters

For a self-centering system that can be represented by a flag-shaped hysteresis, there are four independent parameters: initial stiffness k_0 , linear limit f_y , nonlinear stiffness αk_0 , and energy dissipation parameter β as shown in Fig. 2.1.

The following sections describe how each parameter is normalized in this study. The range of normalized parameters considered in this study is summarized in Table 2.1.

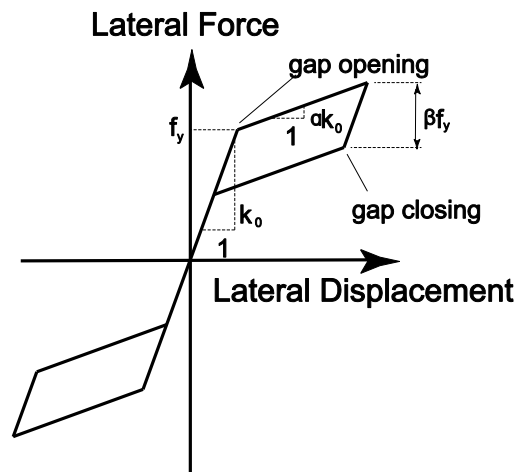


Figure 2.1 Flag-shaped hysteresis

2.1.1 Initial Period

To normalize the results, the initial stiffness k_0 is expressed in terms of the initial

period:

$$T_0 = 2\pi \sqrt{\frac{m}{k_0}} \quad (2-1)$$

where m is defined as unity.

Table 2.1 Parameters Considered

System Parameter	Values Considered	
Initial Period T_0 (s)	0.05–1.0 (increments of 0.05) 1.0–3.0 (increments of 0.1)	
Tangent Period T_{\tan} (s)	–5, –10, –20, ∞ , 20, 10, 8, 5, 3, 2, 1.5, 1	
Force Reduction Factor R	2, 4, 6, 8, 10, 15, 20, 30, 50, 100	
Hysteretic Energy Dissipation Parameter β	0, 0.1, 0.2, 0.4, 0.5, 0.6, 0.8, 1.0	
Damping Ratio ζ	Initial damping model : 5% , 2% , 10%	Tangent damping model 5%

Some studies on SDOF systems considered an initial period in the range of 0.1–3s (e.g. Miranda 2000, Seo and Sause 2005) as most buildings are in this period range, while other studies considered only 0.25–2.0s (e.g. Christopoulos et al. 2002, Priestley and Grant 2005). In this study, $T_0 = 0.05–3.0s$ is adopted.

The step between $T_0 = 0.05–1.0s$ is 0.05s, while the step between $T_0 = 1.0–3.0s$ is 0.1s. The shorter period step at short periods is because a $T_0 = 0.05–1.0s$ corresponds to buildings of 1–10 storey high based on the estimation of $T_0 = 0.1N$ (N is the number of stories for a building) and this range is relatively common. Also, previous studies on self-centering SDOF systems (e.g. Christopoulos et al. 2002, Seo and Sause 2005) showed that at short periods

($T_0 \leq 1.0s$), the variation of displacement demand changes more rapidly than at longer periods.

2.1.2 Tangent Period

For the nonlinear stiffness term αk_0 , previous studies (Christopoulos et al. 2002, Seo and Sause 2005) used α to relate it to the initial stiffness. However, for self-centering systems, the nonlinear stiffness is normally determined by the post-tensioning, almost independent of the initial stiffness (Wiebe and Christopoulos 2014). When designing a self-centering system, the post-tensioning is normally selected relatively early in design, before the initial stiffness is known. Therefore, this study does not normalize the nonlinear stiffness by the linear stiffness. Instead, the nonlinear stiffness is described by the tangent period, which is defined as:

$$T_{\tan} = 2\pi \sqrt{\frac{m}{|\alpha|k_0}} \times \text{sgn}(\alpha) \quad (2-2)$$

where α is the ratio of nonlinear stiffness to initial stiffness. By this definition the tangent period is negative when $\alpha < 0$, and $T_{\tan} = \infty$ for systems with zero nonlinear stiffness. In addition to being preferable for design, another advantage of this definition is that it separates the nonlinear stiffness completely from the initial stiffness, decoupling these two parameters from a research perspective.

Christopoulos et al. (2002) adopted a nonlinear stiffness ratio of $0.02 \leq \alpha \leq 0.35$ while Seo and Sause (2005) used $0 \leq \alpha \leq 0.2$. Considering the range of initial period that those studies examined and using Eq.(2-2) to convert α into a tangent period, they correspond to a tangent period range of $T_{\tan} = 0.4 - 14s$ and $T_{\tan} = 0.2s - \infty$, respectively. For self-centering systems, as the nonlinear stiffness is provided mostly by post-tensioning, $T_{\tan} < 1.0s$ is assumed to be impractical because of physical limitations in construction. Therefore $T_{\tan} = 1.0s - \infty$ is adopted for the positive nonlinear stiffness and a few negative T_{\tan} values are added in the parametric study to represent cases with a small negative nonlinear stiffness due to the $P - \Delta$ effect.

2.1.3 Force Reduction Factor

The linear limit of the flag-shaped hysteresis is defined in the following way. Assuming an elastic system with infinite strength and its peak force during an

earthquake is $f_{elastic}$, then $\frac{|f_{elastic}|}{R}$ is defined as the linear limit f_y (Fig.2.2), where

$R \geq 1$ and R is called the force reduction factor, which represents how much the design forces are reduced from an elastic design.

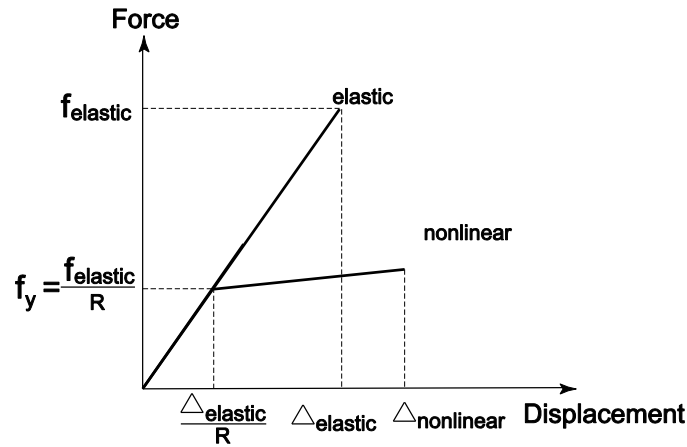


Figure 2.2 Definition of force reduction factor

The current National Building Code of Canada allows a force reduction factor of 1.0–8.0 in seismic design for traditional systems (NRCC 2010). Therefore, when selecting R values for this parametric study, more attention is given to relatively small force reduction factors 2–10 as this is the range that conservative engineers are likely to consider for design. However, it has been suggested that a larger force reduction factor can be used without structural damage in self-centering systems (Wiebe and Christopoulos 2014). One of the main objectives of this study is to explore the effect of large R values on the displacement demands. Thus, a few large values that represent the research ambition to allow larger R are also considered to explore how large R can be if the peak displacement is the only concern.

2.1.4 Hysteretic Energy Dissipation Parameter

The ratio of the height of the flag to the linear limit represents the relative level of

the hysteretic energy dissipation capacity and is termed the hysteretic energy dissipation parameter β (Fig.2.1). To maintain the self-centering feature, it must be ensured that $\beta \leq 100\%$. In previous studies, Christopoulos et al. (2002) used $\beta = 0\%, 30\%, 60\%$ and 100% , Seo and Sause (2005) used $\beta = 0\%, 25\%, 50\%$ and 100% , and Wiebe and Christopoulos (2014) used $\beta = 0\%, 50\%$ and 100% . In this study, more values of β are considered to make the regression more generalized.

2.2 Inherent Damping Model

2.2.1 Initial Stiffness Proportional Damping Model

Most previous studies on the displacements of SDOF systems have modelled the inherent damping with an initial stiffness proportional damping model, where the damping coefficient is defined as:

$$c = 2\zeta \sqrt{mk_0} \quad (2-3)$$

where ζ is the damping ratio.

In practice, a viscous damping ratio of 5% is usually assumed (Chopra 2012). However, uncertainties are associated with the real damping ratio. In addition, different damping values are recommended for structures with different materials. For example, Newmark & Hall (1982) suggested that a damping ratio of 2% can

be applied for steel structures and a damping ratio of $7\% \leq \zeta \leq 10\%$ can be applied for reinforced concrete structures. As self-centering systems can be applied to both concrete and steel structures, it is worthwhile to explore the effect of different damping ratios. Therefore, the damping ratio in the initial stiffness proportional damping model is changed from 5% to 2% and 10% .

2.2.2 Tangent Stiffness Proportional Damping Model

When the system enters the nonlinear range, the initial stiffness proportional damping model keeps the damping term c constant. Therefore, this damping model may create a very large damping force relative to the structural force in the nonlinear range, with potentially unconservative results.

To overcome this problem, a tangent stiffness proportional damping model has been proposed in multi-degree-of-freedom systems (Leger and Dussault 1992). A recent study has explored the difference between an initial stiffness proportional damping model and a tangent stiffness proportional damping model for SDOF systems with various hysteresis loops, including modified Takeda model, bilinear model and flag-shaped model (Priestley and Grant 2005). The tangent stiffness proportional damping model resulted in larger displacements than the initial proportional damping model and was argued to be more realistic. Other research on multi-degree-of-freedom (MDOF) system modelling also

recommended the tangent stiffness proportional damping over the initial stiffness proportional damping (e.g. Charney 2008).

In this study, a separate set of analyses is carried out with the tangent stiffness proportional damping model, which is defined for this work as:

$$c_i = \begin{cases} 2\zeta \sqrt{mk_{i-1}} & k_{i-1} \geq 0 \\ 0 & k_{i-1} < 0 \end{cases} \quad (2-4)$$

where k_{i-1} is the stiffness of the system at previous time step. This stiffness is used instead of the current stiffness to avoid convergence problems caused by iterating the stiffness within one time step. For brevity, the first damping model (Eq.2-3) will be called initial damping model and the second (Eq.2-4) will be called tangent damping model for the rest of the thesis.

2.3 Ground Motion Records

80 unscaled historical ground motion records are used for the main analyses of this study. These records are given as set #1A in PEER transportation research program, selected for stiff soil sites (Baker et al. 2011). They are intended to represent the dominant hazard in active seismic regions with large earthquakes ($M = 7$) at small distances ($10km$). The elastic response spectra are shown in Fig.2.3. A sample ground motion that is close to the median response spectrum is highlighted here and is used for time history analysis examples in this thesis.

Another set of ground motions that is representative of the same hazard level, but for rock site conditions (set #2 in Baker et al. 2011), is also used for another set of analyses. The ground motion records listed by Baker et al. (2011) were downloaded from PEER website (PEER 2011).

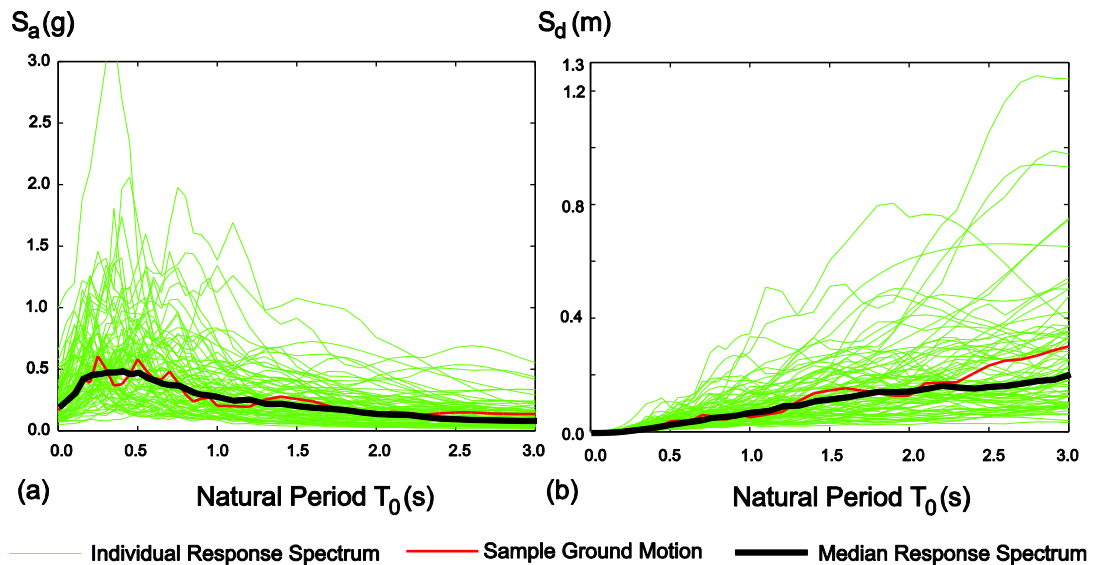


Figure 2.3 Ground motion records: a) acceleration spectra; b) displacement spectra

In this study, the parameters are normalized in such a way that the scaling of ground motions does not affect the results. This is because the linear limit of the system (f_y in Fig.2.1(a)) for each nonlinear time history analysis is defined as the peak elastic force demand for that record divided by R . Therefore, the ground motion scaling has the same effect on both the demand and the capacity, resulting into no change to the normalized results. For example, scaling the ground motion by a factor of 2 will increase both the elastic displacement and the

nonlinear displacement by a factor of exactly 2. Therefore, when the results are normalized by the elastic displacement (see Section 2.5), they will not change due to the scaling of ground motions.

2.4 Numerical Solution Technique

All of the results in this thesis are obtained by programs written by the author in MATLAB (MathWorks 2014a). The linear and nonlinear time history analyses are carried out using Newmark's method with constant average acceleration ($\gamma = 0.5, \beta = 0.25$) and Newton-Raphson iteration (Chopra 2012). The tolerance of iterated forces as convergence criteria in the scheme is 0.001. This tolerance is small enough to ensure accurate results: a smaller tolerance (10^{-6}) produces results that are mostly the same in the first 5 digits except all leading zeros (in the order of $0.01mm$). The maximum number of iterations is 1000 times, after which the analyses will be stopped. Because the hysteresis is defined by straight lines, convergence could normally be achieved within 5 iterations. Non-convergence was not observed for systems with a zero or positive nonlinear stiffness and $T_0 \geq 0.2s$. Based on checking several analyses that did not converge 1000 steps, non-convergence always indicated collapse for the reasons that are discussed later in Section 3.1.1.

For all analyses, a zero ground acceleration point is added at the beginning of each record and 5s of zero ground acceleration is added at the end of each original record to allow enough free vibration in case that a peak displacement occurs after the recorded time. The time step for elastic and nonlinear time history analyses is selected as $\Delta t = 0.001s$, and the ground accelerations are divided into a time step of 0.001s by linear interpolation. Time steps of 0.01s, 0.005s, 0.001s, 0.0005s and 0.0001s were also considered for sensitivity checks. It is found that after 0.001s, as the time step becomes shorter, the results change by less than 0.1% for $T_0 = 0.2s$, and by even smaller amounts for longer initial periods. Based on these analyses, the time step of $\Delta t = 0.001s$ is short enough to give accurate results.

Some analyses were carried out to check the code against previous studies (Christopoulos et al. 2002) and some unpublished mutually independent work and reached good agreement. The results are summarized in Appendix A.

2.5 Analysis Example

Using the sample ground motion shown in Fig.2.3, time history analyses for both the elastic and a corresponding nonlinear SDOF systems are carried out and shown in Fig.2.4(a) and Fig.2.4(b). The elastic system in this example has $T_0 = 0.5s$ and the nonlinear system has $T_0 = 0.5s$, $R = 4$, $\beta = 0.5$ and $T_{\tan} = \infty$.

Each system is assigned a unit mass. Fig.2.4(a) shows the time history response of the two systems and that the vibration period of the nonlinear system is longer than the elastic system even though their initial periods are the same. Fig.2.4(b) shows the hystereses of the two systems and proves that the nonlinear model works well to capture the flag-shaped hysteresis.

Repeating similar analyses for all 80 ground motions, the nonlinear peak displacements for the self-centering system are drawn in Fig.2.5(a).

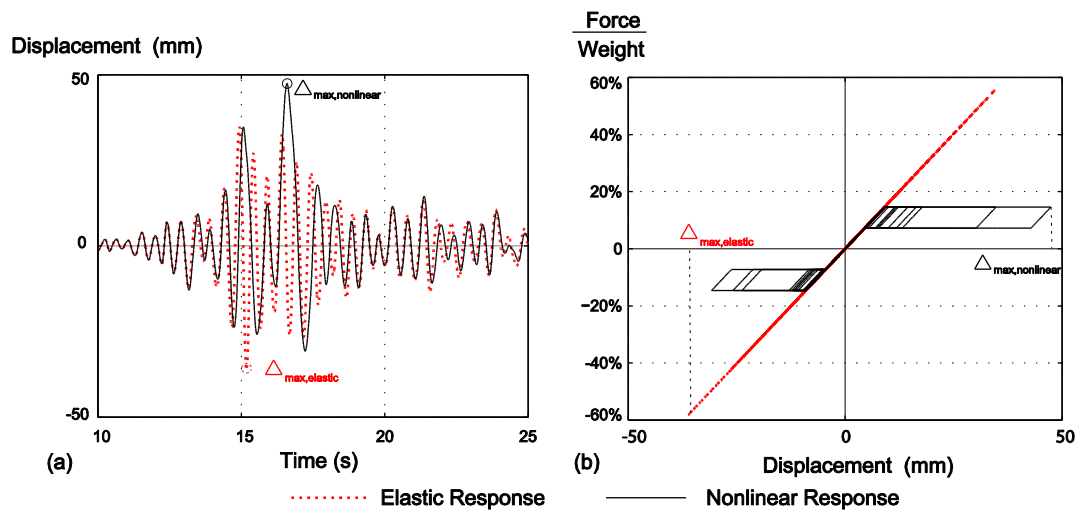


Figure 2.4 Example Analyses: a) time history; b) hysteresis

To normalize the results, the displacement coefficient is defined by Eq.(2-5).

$$C_R = \left| \frac{\Delta_{\max, \text{nonlinear}}}{\Delta_{\max, \text{elastic}}} \right| \quad (2-5)$$

By this definition, the peak nonlinear displacements of the self-centering systems are normalized by the peak displacement of an elastic system with the same initial period (e.g. Fig.2.4(b)).

Note that in all of the following figures, $C_R = 1$ stands for the equal displacement assumption and $C_R > 1$ means that the equal displacement assumption is unconservative. The results of C_R for this example are shown in Fig.2.5(b).

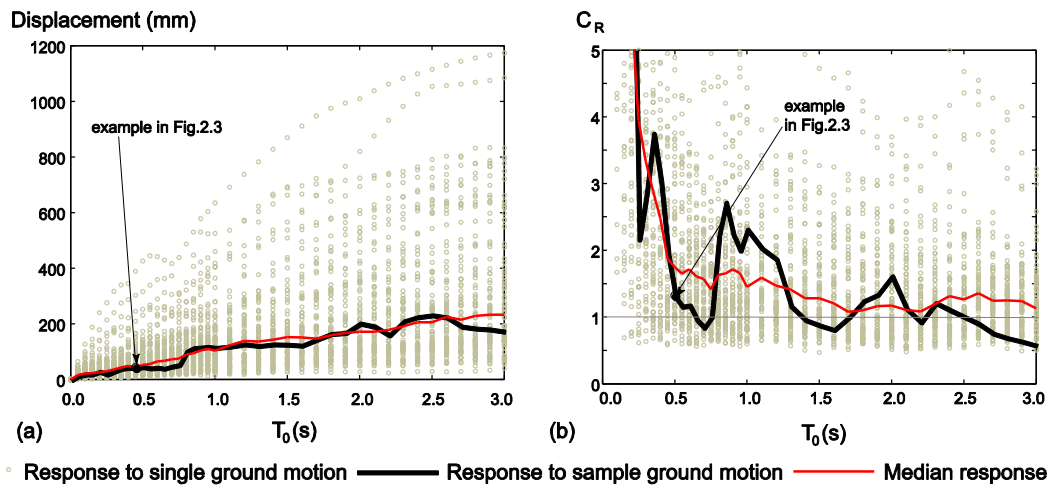


Figure 2.5 Example Analyses: a) individual and median displacement; b) individual and median displacement coefficient

As can be seen from Fig.2.3 and Fig.2.5, the response of both linear elastic and self-centering systems are highly variable, even for a set of ground motions with similar magnitude and distance. However, the variability of the nonlinear response is not the same as the variability of the elastic spectra. For instance, both the elastic acceleration spectrum and the elastic displacement spectrum of the sample ground motion at $T_0 = 0.5s$ are slightly larger than the median values.

Conversely, the nonlinear displacement in Fig.2.5(a) is slightly smaller than the median value, and the displacement ratio in Fig.2.5(b) is much smaller than the median. This indicates that the variability in C_R is not only because of the variability in elastic spectra at the initial period.

In earthquake engineering practice, seismic responses are usually assumed to follow a lognormal distribution (Abrahamson and Silva, 1997, Boore et al. 1997, Shome and Cornell, 1999, Seo 2005). Therefore, the counted median value is preferred to represent the average because it corresponds to a 50% probability of exceedance, whereas the mean value leads to a systematically larger value.

In this study, unless stated otherwise, the results and discussion are expressed in terms of median displacement coefficient. The 84th percentile results are discussed in Section 3.3.

CHAPTER 3: RESULTS OF PARAMETRIC STUDY

Using the ground motion records from Baker (2011), a statistical parametric study is conducted, consisting of 13,440,000 nonlinear time history analyses, to analyze the influence of different parameters on the displacement demands of self-centering systems. Unless otherwise stated, the following results and discussions are all in terms of median responses.

3.1 Initial Damping Model

3.1.1 Baseline Study

Influence of Initial Period

To investigate the influence of initial period, the tangent period is fixed as $T_{\tan} = \infty$ (zero nonlinear stiffness) and the variation of C_R with respect to T_0 is shown in Fig.3.1. C_R generally decreases as T_0 increases. For the case of $R = 2$ or $R = 4$, C_R becomes close to constant when $T_0 > 0.5s$. But for larger R values ($R \geq 8$), C_R keeps decreasing with increasing T_0 . The equal displacement assumption ($C_R = 1$) generally underestimates the displacement of a self-centering system, especially when $R \geq 4$ and $R = 2, \beta = 0$. For short initial periods, C_R becomes very large. For example, in the case of $\beta = 50\%$ and $T_0 = 0.1s$,

$C_R = 6.8$ when $R = 2$, $C_R = 30.4$ when $R = 4$ and $C_R = 41$ when $R = 8$. Although the displacement ratio of $C_R = 41$ seems very large, it corresponds to a displacement of 34mm for a 3.5m one-storey structure, which is only 1% of the height and therefore may be acceptable. For the extreme case of $R = 100$ in Fig.3.1, it is observed to have similar or smaller displacement demand compared with that of $R = 30$. This will be discussed in more details subsequently.

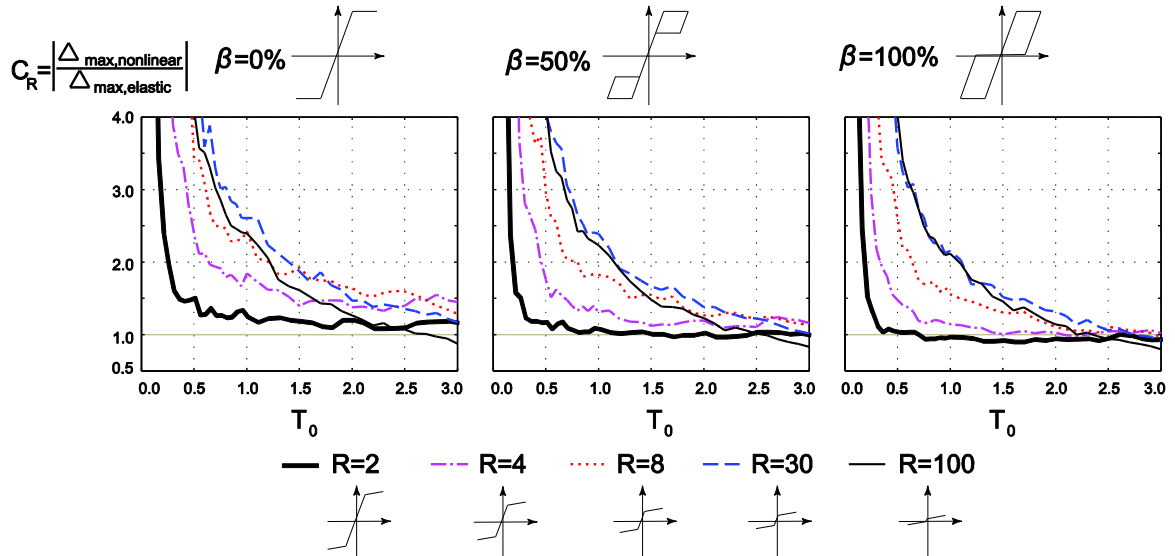


Figure 3.1 Displacement Ratios of Self-Centering SDOF Systems with Respect to Initial Period with Initial Damping Model and $T_{\tan} = \infty$

Influence of Force Reduction Factor

The variation of C_R with respect to R for different combinations of T_0 and T_{\tan} is shown in Fig.3.2. The results for $R = 100$ follow the same trend but are not shown in order to present the results for $R \leq 50$ more clearly. It shows that the value of

C_R is mostly influenced by the initial period T_0 , but C_R generally increases with

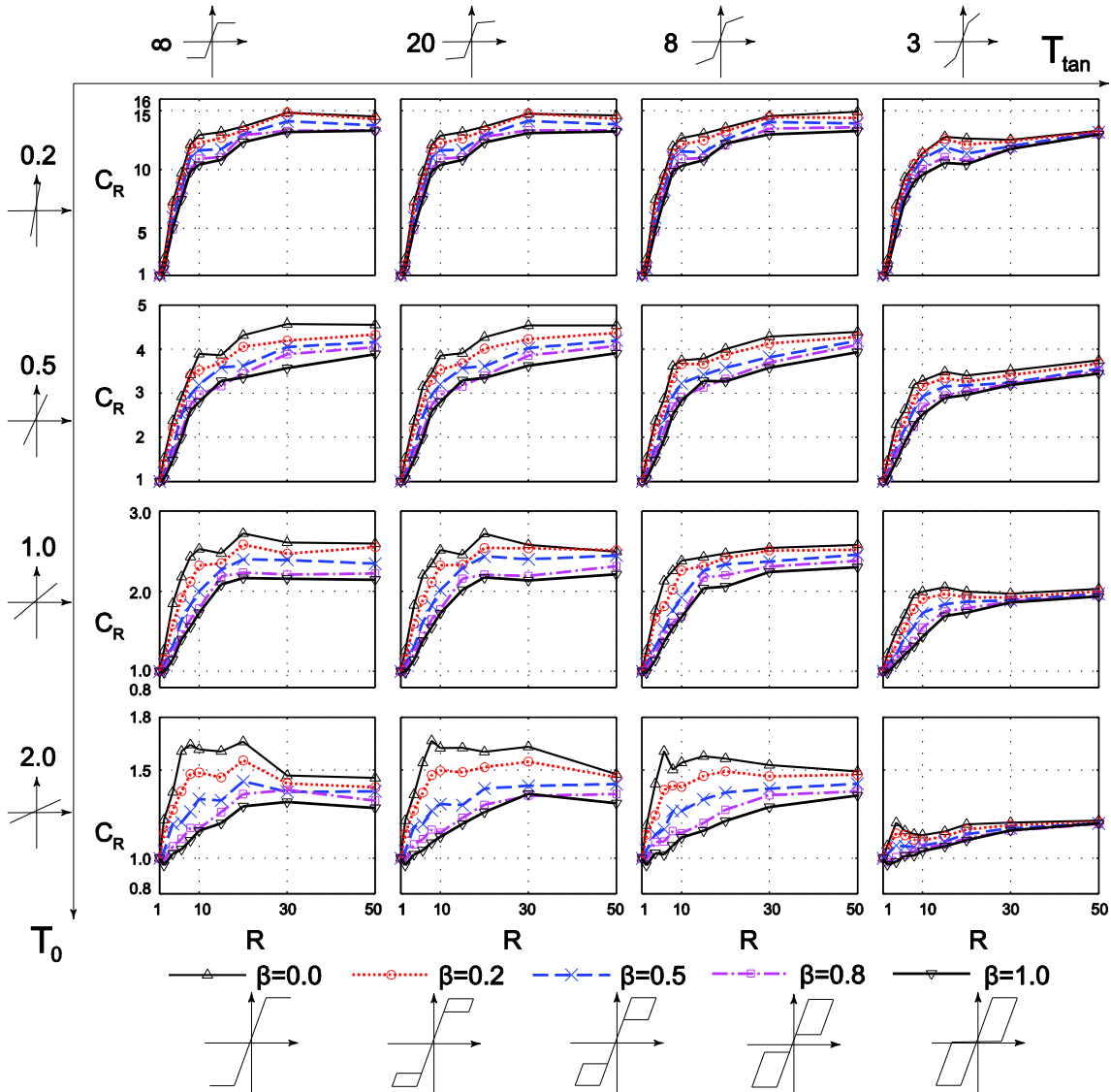


Figure 3.2 Displacement Ratios of Self-Centering SDOF Systems with Respect to Force Reduction Factor with Initial Damping Model

increasing R for systems with different parameters. However, above a critical R value, typically in the range of 15 to 20, C_R stays constant and even decreases

in some cases. When looking at different rows, it can be seen that the influence of R diminishes as T_0 becomes longer. For example, in the case of $T_0 = 0.2s$, $T_{\tan} = \infty$ and $\beta = 1.0$, C_R changes from 2 to 13 when R is increased from 2 to 30. However, if $T_0 = 2.0s$ with the same T_{\tan} and β , C_R only increases from 0.96 to 1.32 when R is increased from 2 to 30.

One surprising observation is that in Fig.3.2 the response of $R = 50$ is sometimes smaller than that of $R = 30$. Also in Fig.3.1, the response of $R = 100$ is smaller than that of $R = 30$ and sometimes even smaller than that of $R = 8$. One possible explanation is that when $R \geq 50$, the vibration period is usually determined by the tangent period of the system rather than initial period, as shown in Fig.3.3(a). This results in an apparent period elongation as shown in Fig.3.3(b). However, the historical records used for the study were selected from PEER database (PEER 2011), which is pre-processed to have a usable bandwidth of 0.01–10s (Ancheta et al. 2013). In Fig.3.3, the system with $R = 100$ spends most of its response history in the nonlinear range, when $T_{\tan} = 20s$, which is outside of this bandwidth. The overall behavior of the whole system is a combination of the response when $T_0 = 0.5s$ and when $T_{\tan} = 20s$, but the response of the system may not be reliable when $T_{\tan} = 20s$. Despite this potential concern, results are presented for large values of R because this range is of interest in the development of self-centering systems (e.g. Wiebe and Christopoulos 2014).

Also, this issue is not unique to self-centering systems; traditional yielding systems, as well as base isolation systems also experience period elongation.

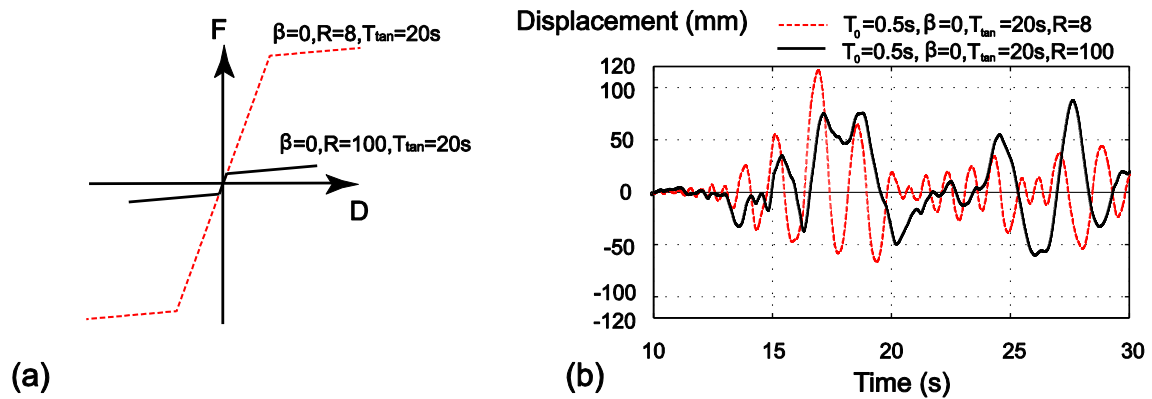


Figure 3.3 Effect of Extremely Large Force Reduction Factor: a) Hysteresis Shape; b) Time History Response

Influence of Hysteretic Energy Dissipation

The energy dissipation parameter β defines the hysteretic energy dissipation that is added to the assumed inherent viscous damping. The changes of C_R with respect to β are shown in Fig.3.4. By comparing different lines, it is clear that T_0 has the greatest influence on C_R . For example, when $T_0 = 0.2s$, $T_{tan} = \infty$ and $R = 8$, C_R varies between 13 and 10 for different β , but when $T_0 = 1.0s$ with the same T_{tan} and R , C_R is only in the range of 1.4–2.0.

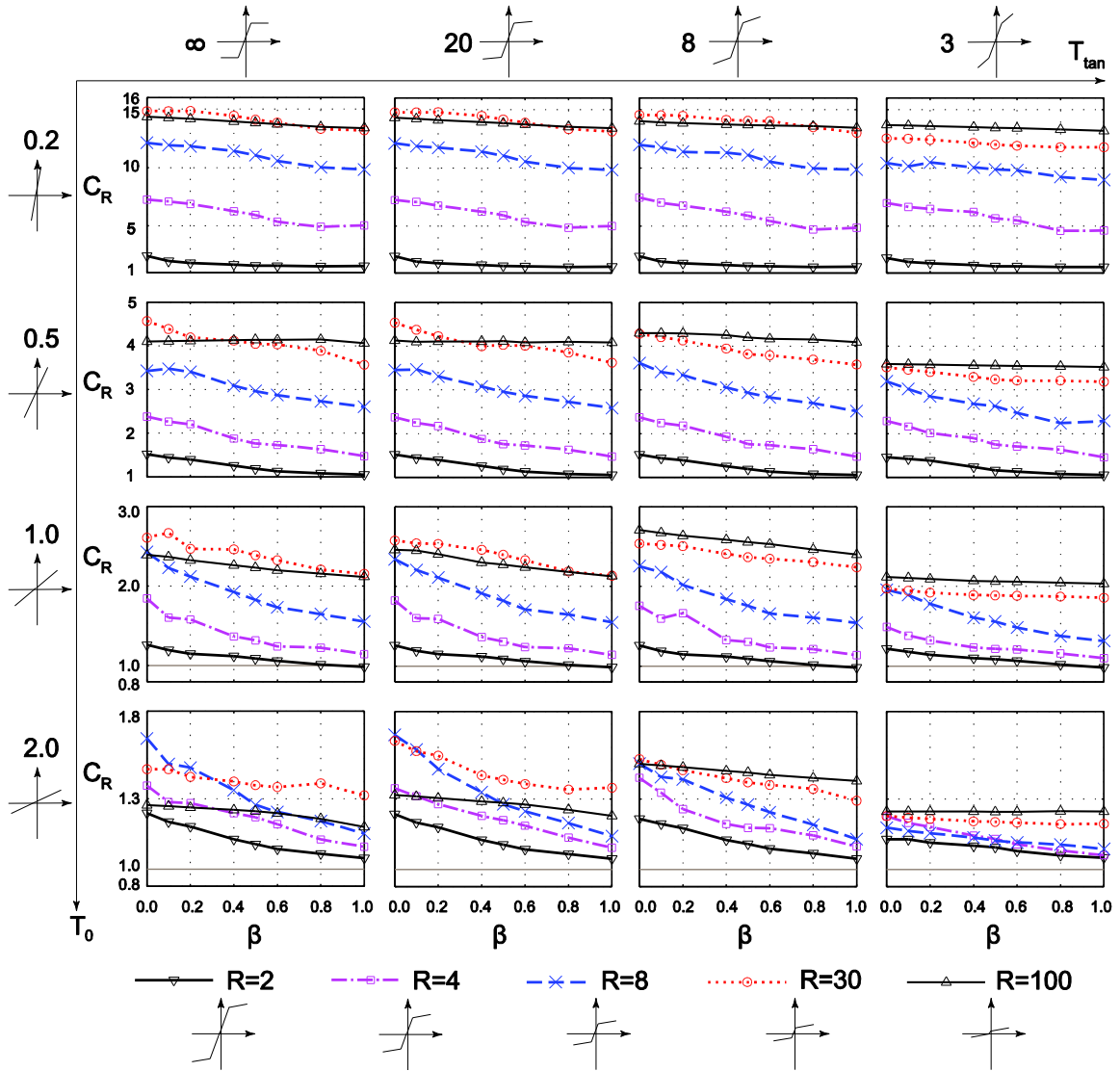


Figure 3.4 Displacement Ratios of Self-Centering SDOF system with Respect to Hysteretic Energy Dissipation Parameter with Initial Damping Model

Generally, C_R decreases as β is increased. However, the curve becomes less steep as β becomes larger. This shows that there are diminishing returns with β : adding energy dissipation to a system with $\beta=0$ has more effect than adding further energy dissipation to a system that already has $\beta > 0$. For example, when

$T_0 = 1.0s$, $T_{tan} = \infty$ and $R = 8$, increasing β from 0 to 0.5 decreases C_R from 2.4 to 1.8 but further increasing β to 1.0 only decreases C_R to 1.6.

Influence of Nonlinear Period

Fig.3.5 shows the variation of C_R with respect to T_{tan} . Generally, when $T_{tan} > 0$, C_R decreases as T_{tan} decreases. This means that as more post-tensioning stiffness is added, the displacement of a self-centering system is suppressed. However, T_{tan} cannot be shorter than T_0 , otherwise the gap-opening will not initiate and the response will be elastic with a constant period of T_0 . And also since there are limitations for the post-tensioning due to constructability, T_{tan} cannot be very close to T_0 .

In Fig.3.5 for $5s \leq T_{tan} < \infty$, the changes of C_R for most systems are mostly within 10%. For example, when $T_0 = 0.5s$, $R = 8$ and $\beta = 0.2$, C_R decreases from 2.1 to 2.0 when T_{tan} decreases from ∞ to $5s$. Exceptions are some cases where $\beta = 0$ or $R = 100$. For the cases where $\beta = 0$, the nonlinear period has a bigger influence than for $\beta > 0$. This is similar to previous findings (Christopoulos et al. 2002, Seo and Sause 2005). For cases where $R = 100$, C_R often increases as T_{tan} decreases from ∞ to $5s$. One possible explanation is that the response of these systems is controlled by the nonlinear period (e.g. $T_{tan} = \infty$), but the ground mo-

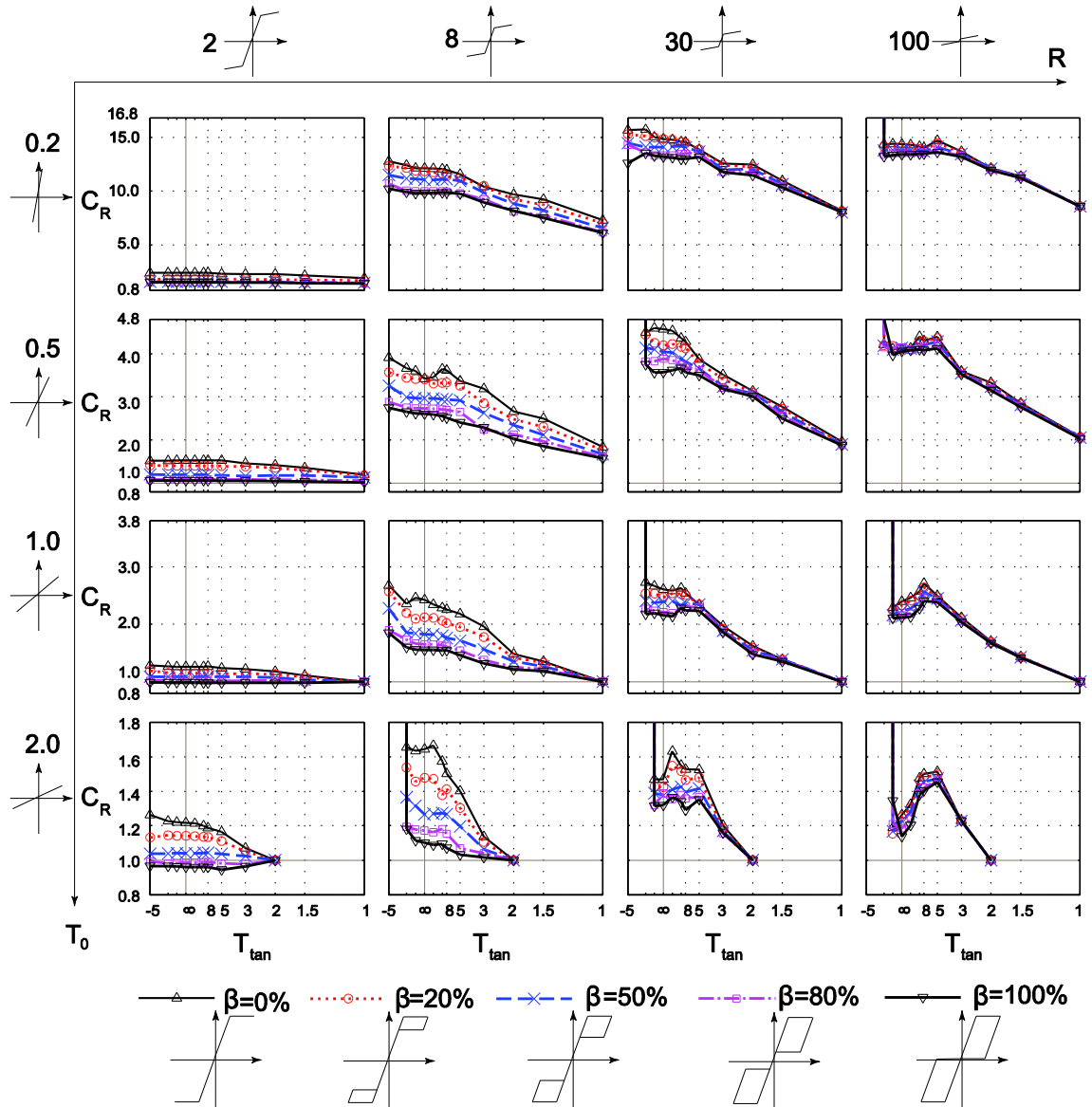


Figure 3.5 Displacement Ratios of Self-Centering SDOF System with Respect to Tangent Period with Initial Damping Model

-tions may not be reliable in these situations as discussed previously. So in general changes of C_R when $5s \leq T_{tan} < \infty$ are negligible. For smaller values of T_{tan} (i.e. $T_{tan} < 5s$), the displacement ratio reduces more significantly. However, such a

large nonlinear stiffness may not be achievable in practice because of the large amount of post-tensioning that would be required.

When T_{\tan} becomes negative and shorter, C_R starts increasing drastically and sometimes becomes a vertical line ($C_R \rightarrow \infty$) in Fig. 3.5. When there is a vertical line in Fig.3.5, it is not because the elastic displacement is very small, since this effect is already reflected by the larger scale of the axis for short-period structures. Rather, a vertical line means that the system may experience large nonlinear displacement and become unstable, resulting in structural collapse. At short initial periods, collapse only happens when R is extremely large ($R=100$ in this case) where $C_R \geq 10^3$ when $T_0 = 0.2s$ in Fig 3.5. The top row of Fig.3.5 shows that self-centering systems with small values of R can still achieve a stable response, even if the displacement ratio is larger than it is for structures with longer initial periods. But as the initial period becomes longer, collapse could happen at smaller R values (i.e. $R=8$ for $T_0 = 2.0s$). This observation can be explained by referring to Fig.3.6. The physical meaning of this collapse is that the system enters the fourth quadrant of its force-displacement relationship graph while the displacement still has a tendency of increasing and then the system becomes unstable. When negative T_{\tan} become shorter, it means that the nonlinear slope is steeper so that the system is more likely to enter the unstable fourth quadrant. A larger R value or a longer initial period means a smaller linear

limit, which increases the likelihood that the system will enter the unstable area in its nonlinear range. Previous research on traditional systems with an elastoplastic hysteresis or a hysteresis that captured strength degradation reached similar conclusions (FEMA 440A).

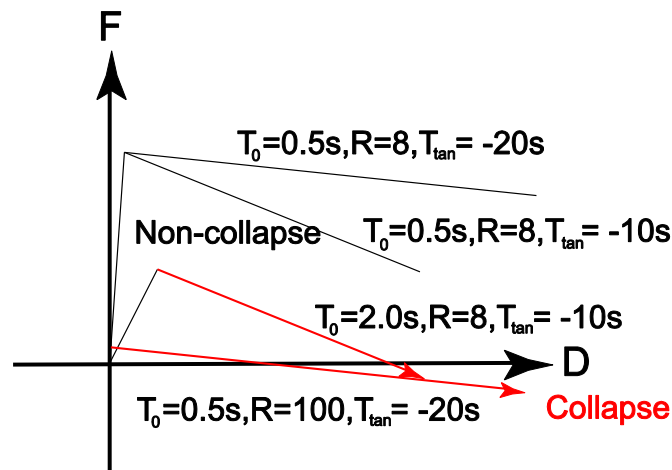


Figure 3.6 Collapse Mechanism

3.1.2 2% and 10% initial damping

This section considers different levels of assumed inherent damping. In these analyses, the linear limit of the self-centering system is calculated from the force demand on an corresponding elastic SDOF system with the same initial period and damping ratio.

When $\zeta = 2\%$ or $\zeta = 10\%$, the general trends of C_R with respect to T_0 , R , β and T_{tan} are similar to those that have already been discussed for $\zeta = 5\%$. So here the

focus is to emphasize the relative difference in C_R compared to $C_{R,5\%}$. Fig.3.7 show the difference between the results with $\zeta = 2\%$ ($C_{R,2\%}$) and those with $\zeta = 5\%$ ($C_{R,5\%}$), normalized by $C_{R,5\%}$. Similarly, Fig. 3.8 show the difference between the results with $\zeta = 10\%$ ($C_{R,10\%}$) and those with $\zeta = 5\%$ ($C_{R,5\%}$), normalized by $C_{R,5\%}$. Values smaller than zero represent a smaller displacement coefficient than with $\zeta = 5\%$, not necessarily a smaller displacement.

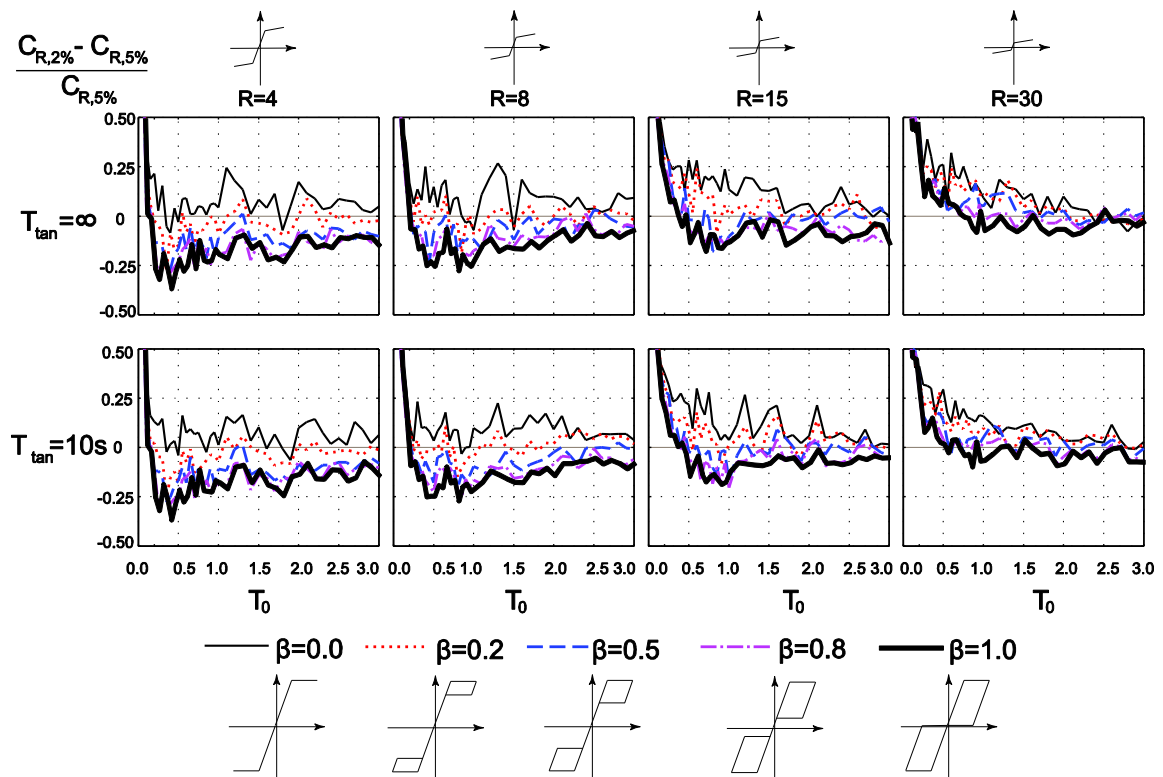


Figure 3.7 Relative Difference of Displacement Ratios between 2% and 5% Damping Ratio

Fig.3.7 shows that a smaller damping ratio usually results in larger C_R when the hysteretic energy dissipation is small (e.g. $\beta = 0, \beta = 0.2$), while it usually leads to smaller C_R when the hysteretic energy dissipation is relatively large (e.g. $\beta = 0.8, \beta = 1.0$).

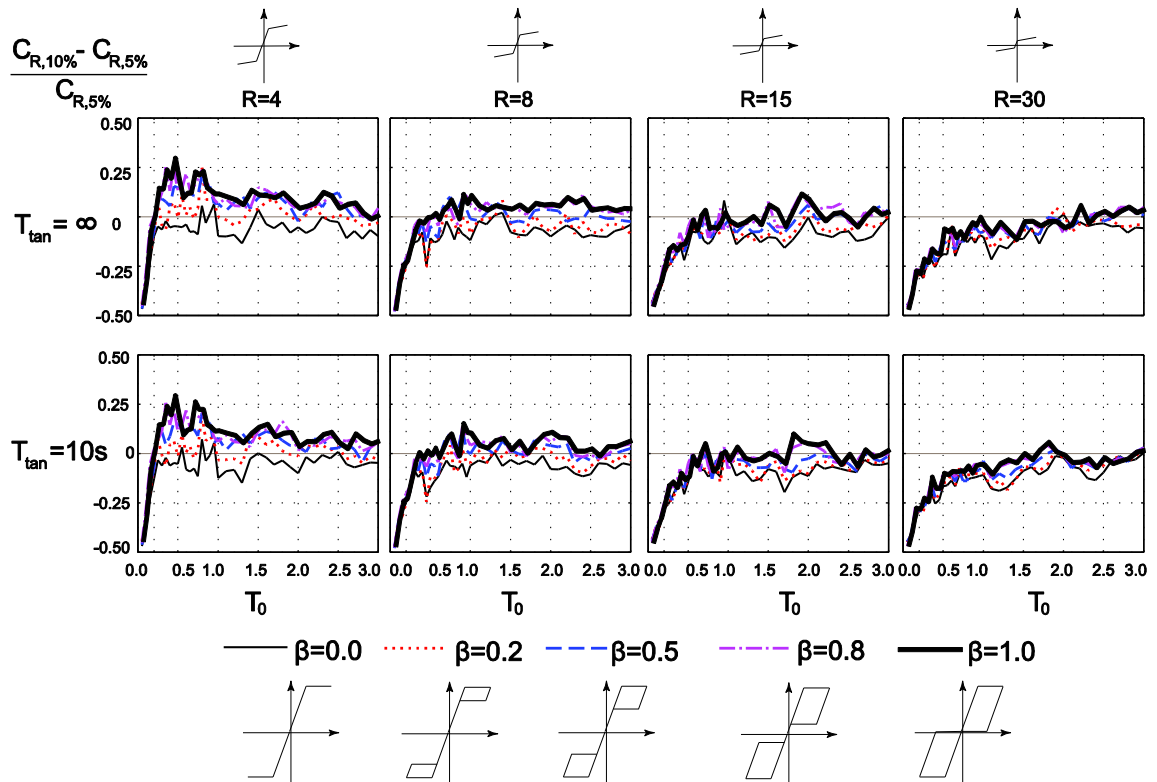


Figure 3.8 Relative Difference of Displacement Ratios between 5% and 10% Damping Ratio

Similarly, the results observed for the difference between 5% and 10% damping in Fig.3.8. Reversely, a larger damping ratio usually results in larger C_R when the

hysteretic energy dissipation is large (e.g. $\beta = 0.8$, $\beta = 1.0$) while it leads to larger displacement ratios when the hysteretic energy dissipation is small (e.g. $\beta = 0$, $\beta = 0.2$). One additional observation is that the differences in C_R for different β values are much smaller than that between 2% and 5% damping. For example, in the case of $T_{\tan} = \infty$, $R = 8$, the value of $\frac{C_{R,10\%} - C_{R,5\%}}{C_{R,5\%}}$ is changed by 0.11 when β is changed from 0 to 1, while the value of $\frac{C_{R,2\%} - C_{R,5\%}}{C_{R,5\%}}$ is changed by 0.40 when β is changed from 0 to 1. Note that the relative difference in C_R between $\zeta = 2\%$ and $\zeta = 5\%$ or $\zeta = 10\%$ and $\zeta = 5\%$ are mostly within 25% , except for $T_0 < 0.2s$.

3.1.3 Ground Motions Recorded on Rock Sites

This section considers another set of ground motions that are representative of the same hazard level (i.e. magnitude and distance) but recorded on rock site conditions. The interest here is how the displacement demands will change if the site condition is changed from a stiff soil site to a rock site. Therefore, Fig.3.9 shows the ratio of the median displacement coefficient that is calculated from the rock site records to the median displacement coefficient that is calculated from soil site records (i.e. $\frac{C_{R,rock}}{C_{R,soil}}$). Compared with the results from soil site records, rock site records lead to a systematically lower C_R value, especially at short

periods. For example, in the case of $R=8$, $T_{\tan}=10s$ and $T_0=0.5s$, $C_{R,Rock}$ is less than 50% of $C_{R,Soil}$. The relative difference between $C_{R,Rock}$ and $C_{R,Soil}$ is almost the constant for all values of β .

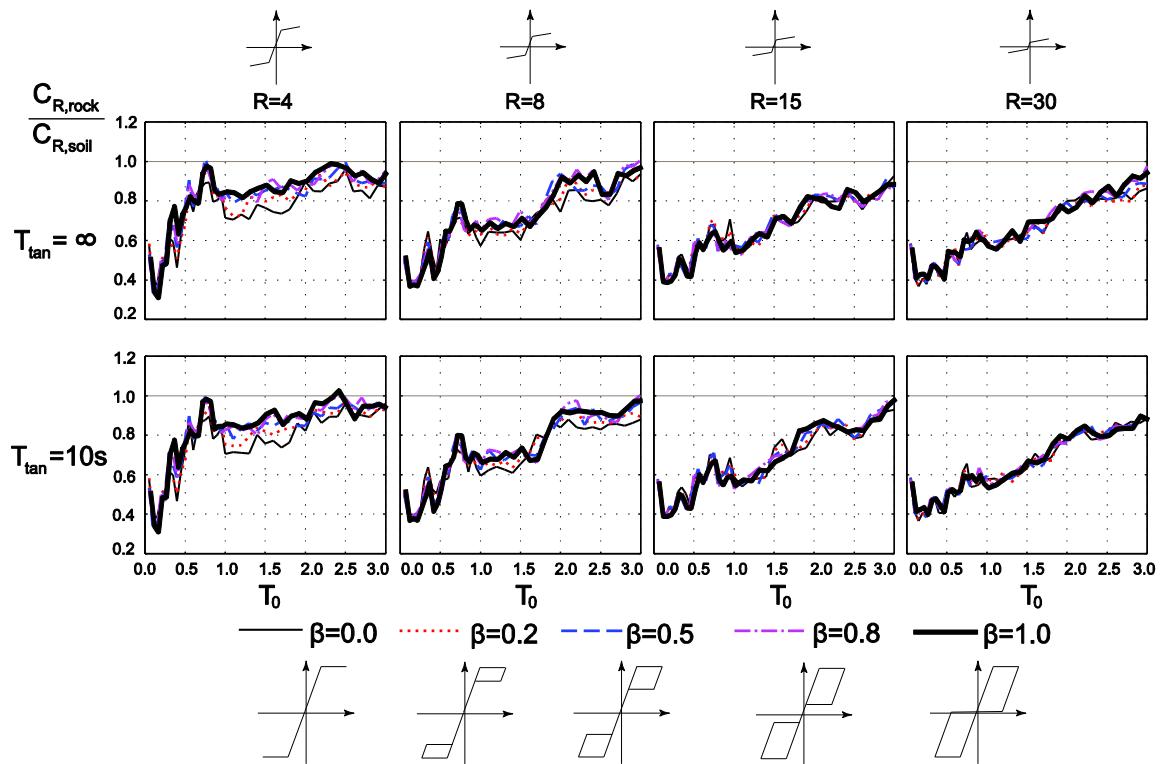


Figure 3.9 Comparison of Displacement Ratios on Rock Sites and Stiff Soil Sites

This observation is generally consistent with the results of a previous study on self-centering SDOF systems (Seo and Sause, 2005). That study concluded that the ductility demand is 50% smaller for ground motions recorded on rock sites than for ground motions recorded on stiff soils sites when $T_0 < 1.25s$ and 30% smaller when $T_0 > 1.25s$. However, here the observation is different. In Fig 3.9,

the displacement demands of self-centering SDOF systems for ground motions recorded on rock sites is about 50% smaller than for ground motions recorded on stiff soil sites only for $T_0 < 0.5s$. The difference between these two decreases linearly with increasing T_0 to about 10% for $R \geq 15$ while for $R \leq 8$ the difference decreases first and then stays constant after a critical T_0 , which depends on the value of R .

These observations on self-centering SDOF systems are different from the conclusion of a previous study on traditional SDOF systems with an elastoplastic hysteresis, which stated that the difference between displacement demands on rock sites and stiff soil sites are within 10% and can be neglected for design purposes (Miranda 2000).

3.2 Tangent Damping Model

3.2.1 Problem with Initial Damping Model

As noted earlier, the assumption of the initial damping model, where the damping coefficient c is a constant according to Eq.(2-3) needs scrutiny. Fig.3.10 shows the time history for self-centering systems of $T_0 = 0.5s$, $\beta = 0.5$, $T_{\tan} = \infty$ but different R values. When the systems enters the nonlinear range, keeping c as a constant creates a relatively large damping force, especially when the linear limit

is low (large R value). For example, in the case of $R=10$, the peak damping force is 58% of the structural force, and in the case of $R=20$, the peak damping force is even larger than the structural force. Note that the plateaus in Fig.3.10 are because of the zero nonlinear stiffness.

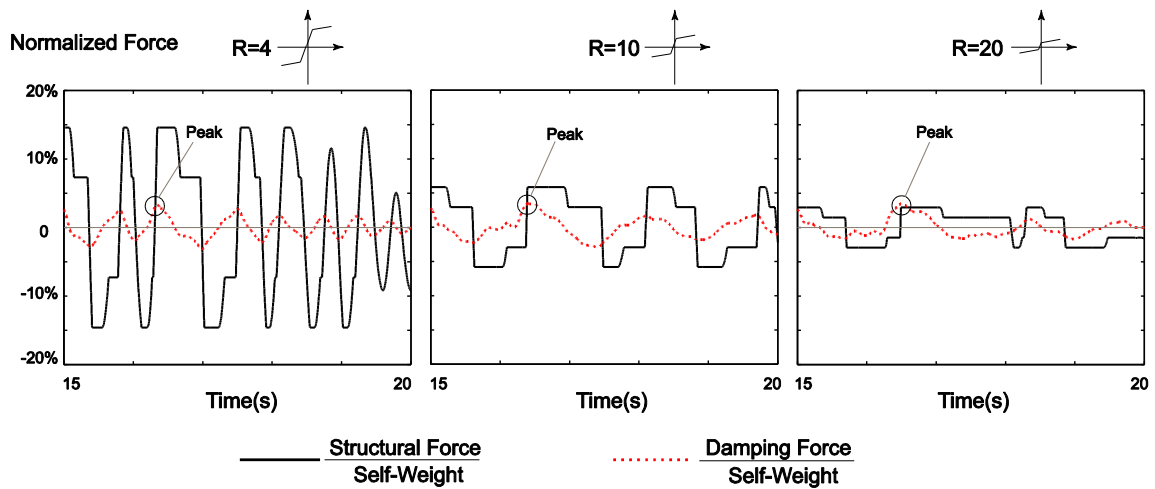


Figure 3.10 Comparison of Structural Force and Damping Force for $T_0 = 0.5s$,

$$\beta = 0.5 \text{ and } T_{\tan} = \infty$$

This phenomenon has also been highlighted in previous studies (Priestley and Grant 2005, Charney 2008), which have suggested using a tangent stiffness proportional damping model instead. The problem of what level of damping force is acceptable is not the focus of this study as more experimental testing is required to determine what the real inherent damping is. Rather, this research focuses on how the displacement demands of self-centering SDOF systems will change, and whether the trends of displacement demands with respect to

different hysteretic parameters will change, if the tangent damping model is used with the same damping ratio of 5% .

3.2.2 Influence of Different Hysteretic Parameters

Influence of Initial Period

Fig.3.11 shows the variation of C_R with respect to initial period, T_0 , when using the tangent damping model. Similar to the trends with the initial damping model, C_R decreases with T_0 . However, compared with Fig.3.1, C_R is much larger, especially when T_0 is small. For example, in the case of $\beta=0.5$ and $T_0=0.1s$, $C_R=16.3$ when $R=2$ and $C_R=130.4$ when $R=4$, the latter of which corresponds to a drift of 3% for a 3.5m tall one-storey structure. These values are 140% and 330% larger when compared to $C_R=6.8$ and $C_R=30.4$ in the previous example when initial damping model is used. If the linear limit is further reduced to $R=8$, then $C_R=214.3$ with the tangent damping model, meaning a drift of 5% . This exceeds the code-specified drift limit of 2.5% (NRCC 2010) and suggest that if self-centering systems are designed for very stiff buildings, the force reduction factor should restricted to small values (e.g. $R=2$).

The only case that the equal displacement assumption is working well within 5% is when $R=2$, $\beta=1.0$ and $T_0 \geq 0.7s$. The scale of Fig.3.11 makes it appear that

C_R is close to 1 at long periods for $R=2$, $\beta=0.5$. But numerical results show that the equal displacement assumption underestimates C_R by more than 10% .

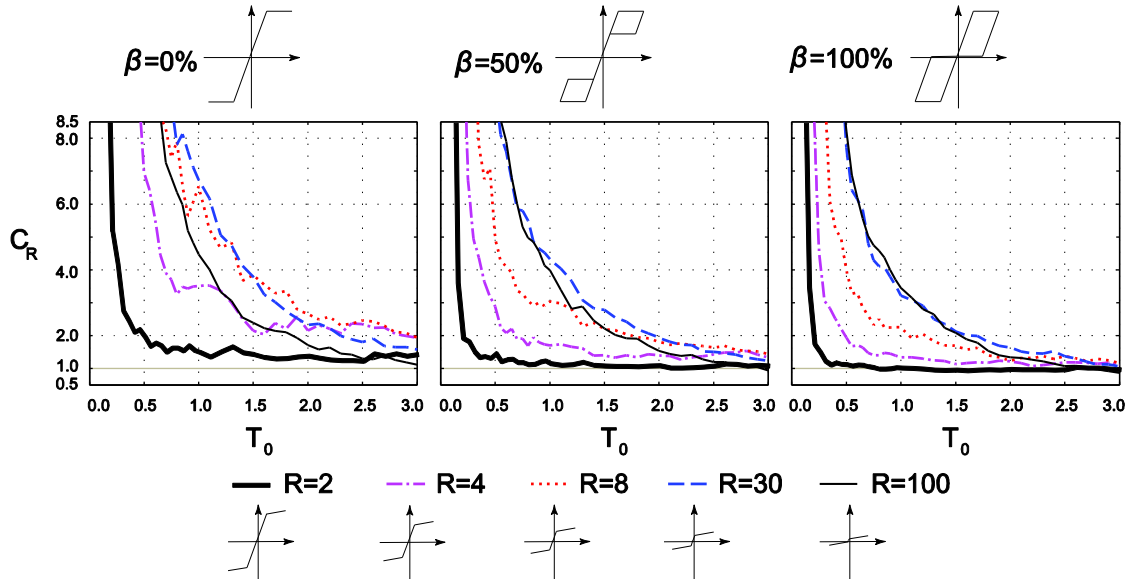


Figure 3.11 Displacement Ratios of Self-Centering SDOF System with Respect to Initial Period with Tangent Damping Model and $T_{\tan} = \infty$

Influence of Force Reduction Factor

Fig.3.12 shows the variation of C_R with respect to the force reduction factor R with the tangent damping model. Compared with the initial damping model, a similar trend of C_R changing with R is observed when R is small, followed by a plateau or decrease above a critical R value. However, significant differences are observed compared with the initial damping model. First of all, the values of C_R are much larger, especially at short initial periods. For instance, in the case of $T_0 = 0.5s$, $T_{\tan} = \infty$, $\beta = 0.5$ and $R = 4$, $C_R = 2.9$ with the tangent damping model,

which is 61% larger than that of the same case when initial damping is used

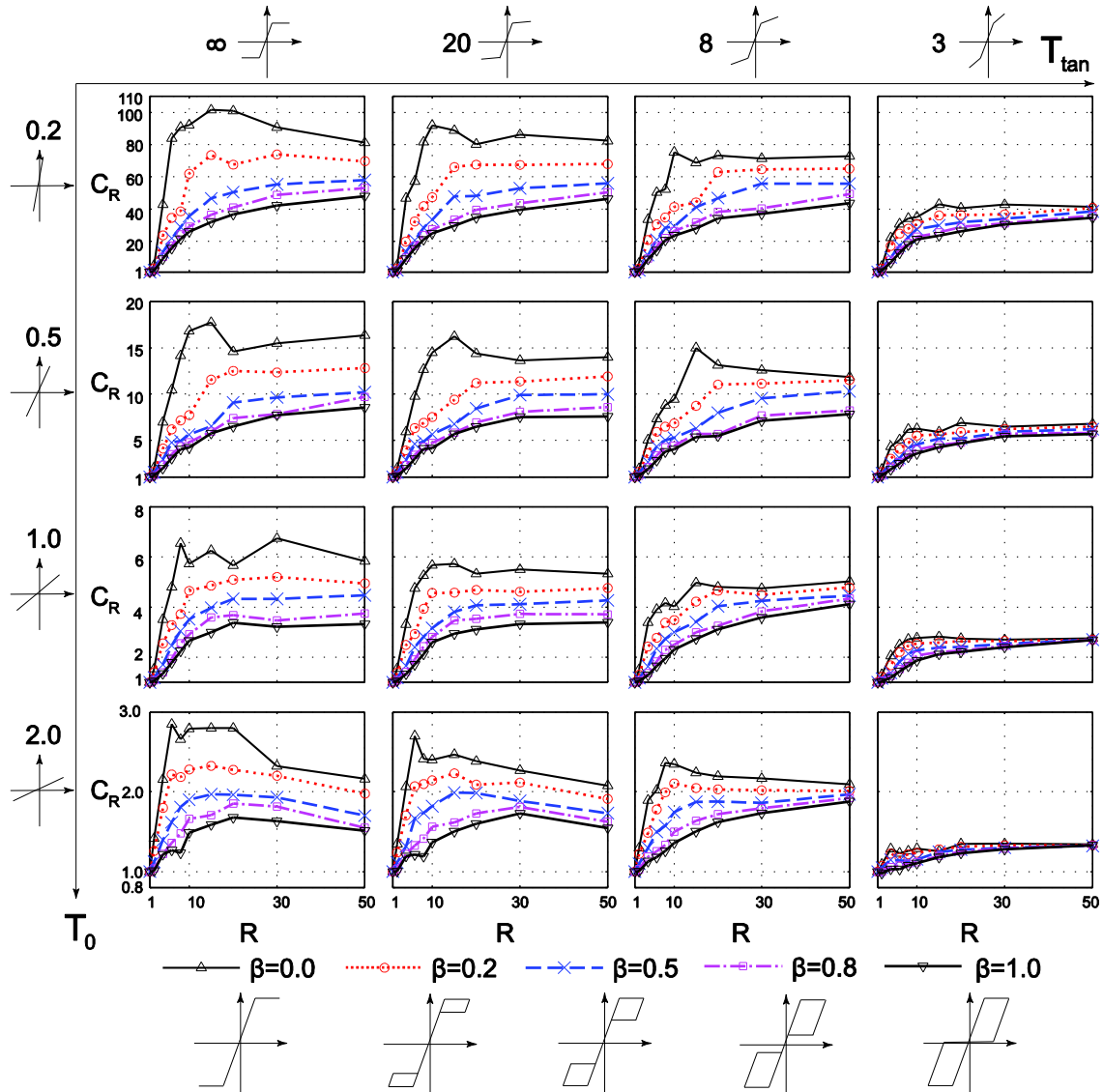


Figure 3.12 Displacement Ratios of Self-Centering SDOF System with Respect to Force Reduction Factor with Tangent Damping Model

($C_R = 1.8$). Also, in the tangent damping model, a shorter tangent period (i.e. a la-

-rger nonlinear stiffness) makes the effect of β less important. This can be observed in Fig.3.12 as in the third column ($T_{\tan} = 8s$), the lines with different β are closer to each other than they are in the first column ($T_{\tan} = \infty$). However, in the initial damping model shown in Fig.3.2, except for the extreme case of $T_{\tan} = 3s$, the distances between different curves with different β are almost the same in the first three columns ($T_{\tan} = \infty$, $T_{\tan} = 8s$ and $T_{\tan} = 20s$).

The observation in Fig.3.12 that the response with $R = 50$ is sometimes smaller than the response with $R = 30$, and the phenomenon in Fig. 3.11 that the response of $R = 100$ is similar or smaller than the response of $R = 30$, can both be explained in the same way as was discussed earlier with the initial damping model.

Influence of Hysteretic Energy Dissipation

Fig.3.13 shows the variation of C_R with respect to β . Compared to the results with the initial damping model (Fig.3.4), the decrease in C_R with increasing β is sharper for small values of β . For example, in the case of $T_0 = 1.0s$, $T_{\tan} = \infty$ and $R = 8$, increasing β from 0 to 50% decreases C_R from 6.5 to 3.0 while the decrease in C_R is only from 3.0 to 2.2 when β is further increased from 50% to 100%.

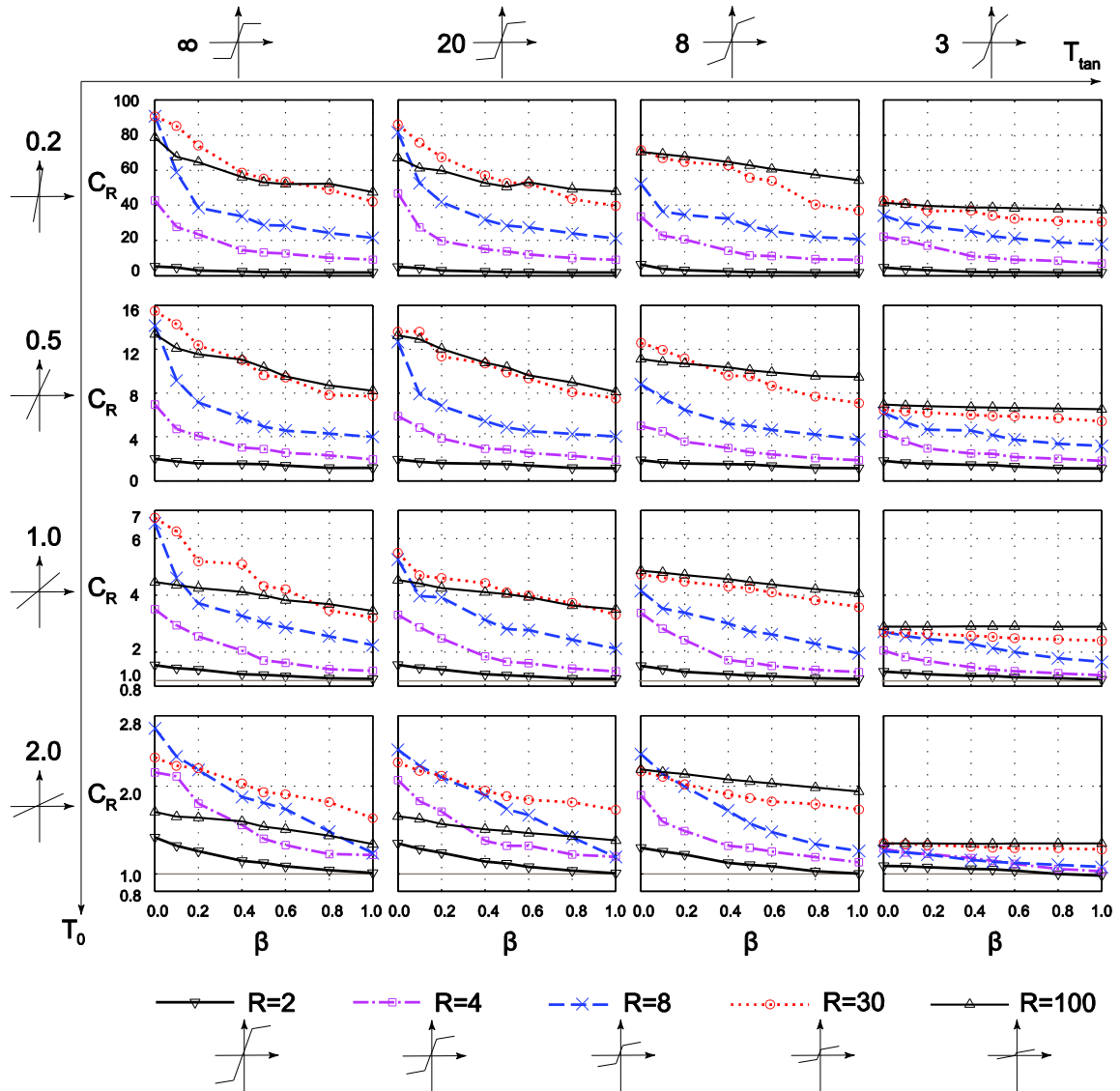


Figure 3.13 Displacement Ratios of Self-Centering SDOF Systems with Respect to Hysteretic Energy Dissipation Parameter with Tangent Damping Model

Influence of Nonlinear Period

The trends of C_R versus T_{tan} with the tangent damping model, shown in Fig.3.14, are generally similar to the trends with the initial damping model, although much larger displacement ratios are observed.

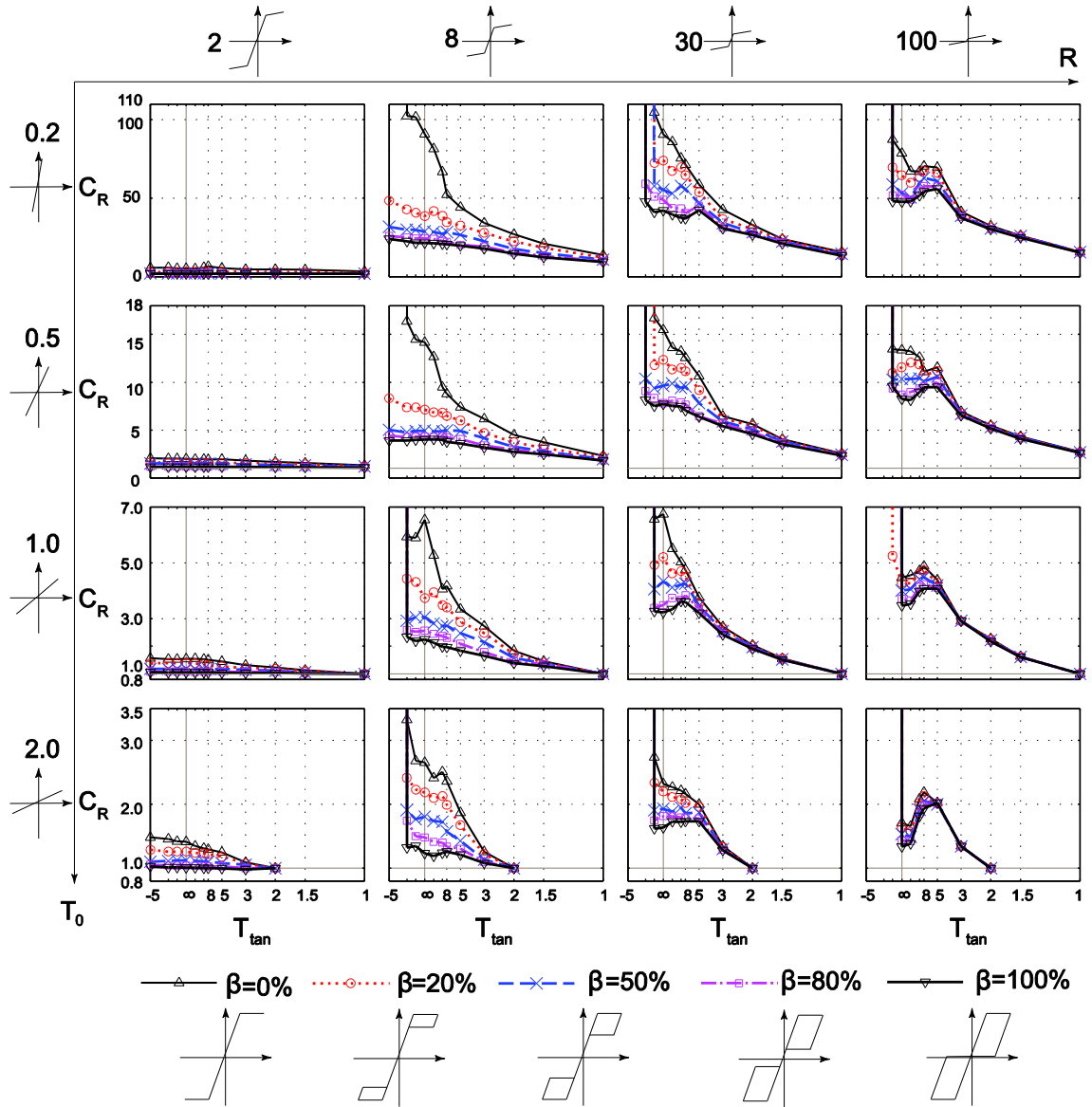


Figure 3.14 Displacement Ratios of Self-Centering SDOF Systems with Respect to Tangent Period with Tangent Damping Model

However, there are some noteworthy differences. First of all, for long tangent periods ($T_{\tan} = \infty - 5s$), Fig.3.14 shows a consistent decrease with increasing T_{\tan} . Even if the slope does not appear to be much steeper than that in Fig.3.5, it is not

negligible because of the scale of vertical axis. For example, in the case of $T_0 = 0.5s$, $R = 8$ and $\beta = 20\%$, the decrease in C_R when T_{\tan} is changed from ∞ to $5s$ is 16%. In contrast, the decrease is only 6% when the other parameters are the same and initial damping model is used. In other words, the post-tensioning is more effective in reducing displacements when the tangent damping model is assumed than when the initial damping model is assumed.

3.3 84th Percentile Displacement Demands

Fig. 2.4 shows that there is a high variability of displacement ratios for systems with same parameters when subjected to different ground motion records. Therefore, it is good to know if the trends of the 84 percentile values with respect to different hysteretic parameters are similar to that of the median. Fig.3.15 shows the relationship between the 84th percentile C_R over 80 ground motions and T_0 . Compared with Fig.3.1 and Fig.3.11, the general trend is the same that the 84th percentile C_R decreases as T_0 increases. The variation of the 84th percentile C_R with R is also similar. For the case of $\beta = 50\%$, $T_0 = 1.0s$ with the initial damping model, increasing R from 2 to 8 increases the 84th percentile C_R from 1.5 to 3.9 but further increasing R from 8 to 30 only changes the 84th percentile C_R from 3.9 to 4.8. For the same case of $\beta = 50\%$, $T_0 = 1.0s$ but with the tangent damping model, increasing R from 2 to 8 increases the 84th

percentile C_R from 1.7 to 8.2 but further increasing R from 8 to 30 only changes the 84th percentile C_R from 8.2 to 9.5.

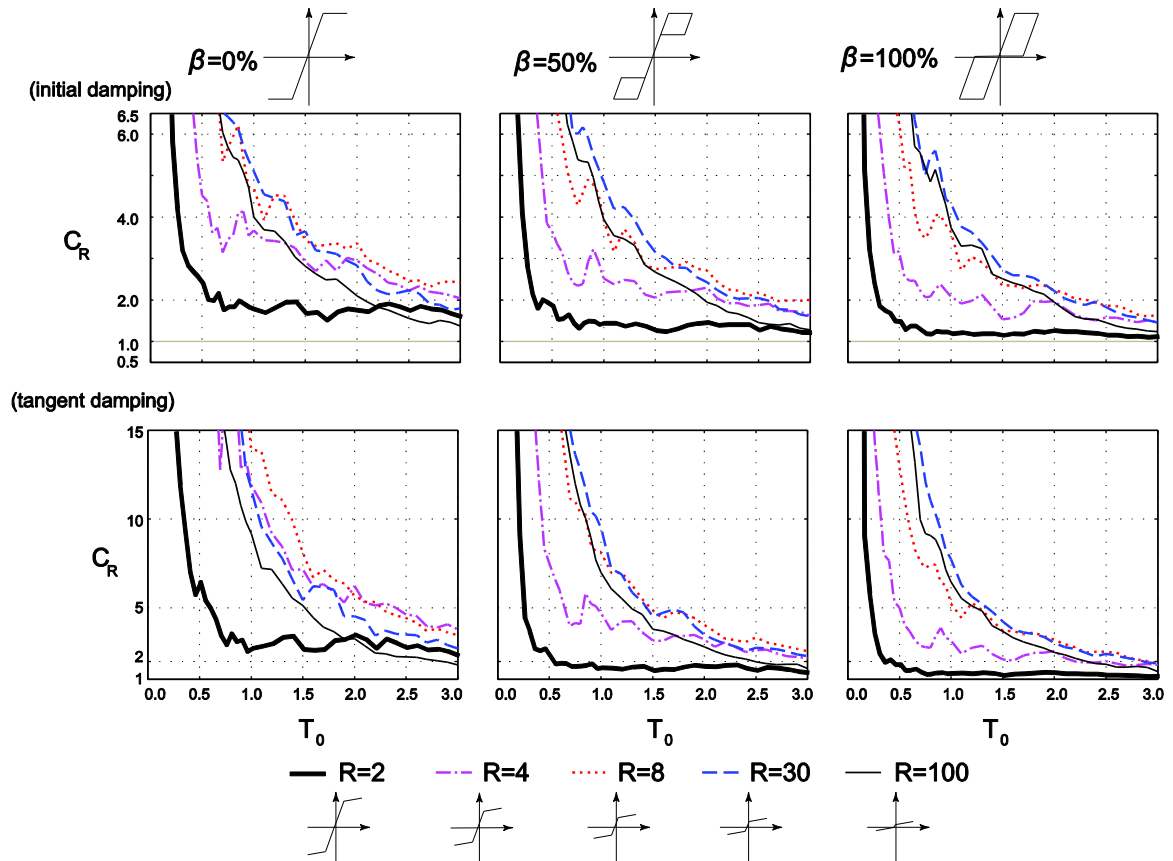


Figure 3.15 84th Percentile Displacement Ratios with $T_{tan} = \infty$

Similar to what was observed for the median results, β has diminishing returns to reduce the 84th percentile C_R as well. For the case of $T_0 = 1.0s$ and $R = 8$ with the initial damping model, increasing β from 0% to 50% decreases the 84th percentile C_R from 4.7 to 3.9 while increasing β from 50% to 100% decreases

the 84th percentile C_R from 3.9 to 3.6. For the same case of $T_0 = 1.0s$ and $R = 8$ but with the tangent damping model, when β is increased from 0% to 50% and then to 100% , the corresponding 84th percentile C_R is decreased from 13.9 to 8.2 and then to 5.2.

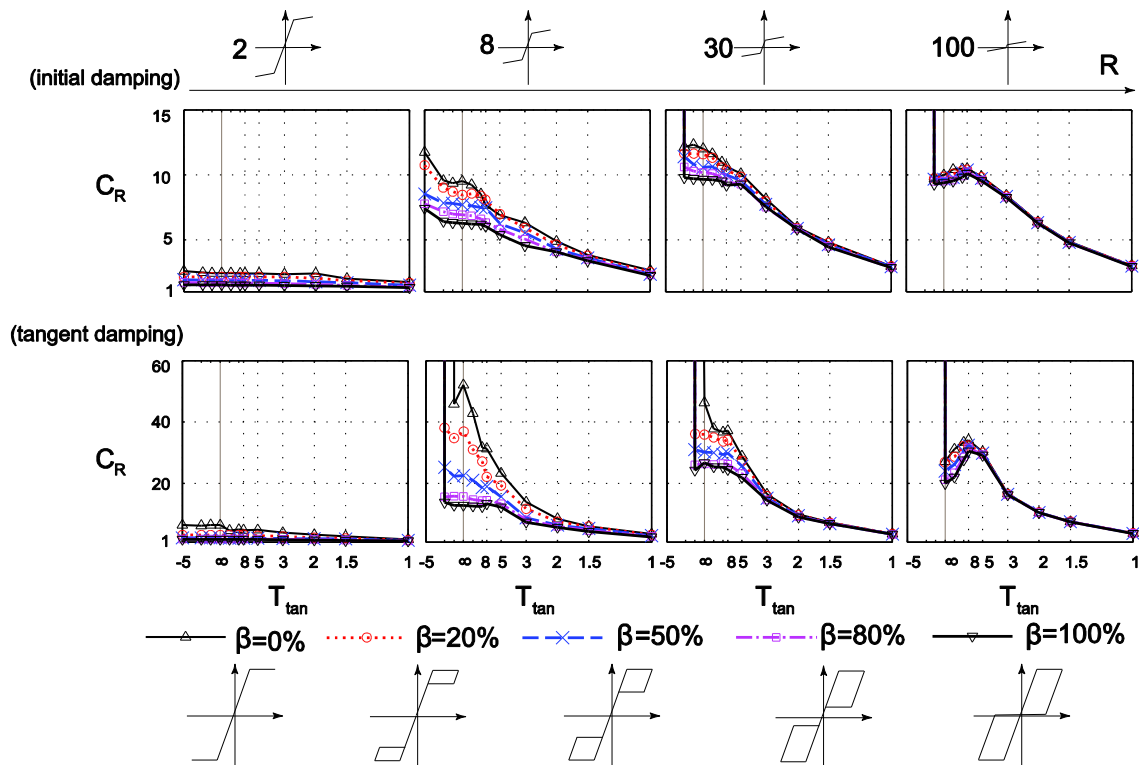


Figure 3.16 84th Displacement Ratios with $T_0 = 0.5s$

The variation of the 84th percentile C_R with respect to T_{tan} is shown in Fig.3.16. As was observed for the influence of nonlinear period on the median C_R , the influence of nonlinear period is more effective for tangent damping model. When

$R=8$ and $\beta=20\%$, the variation of the 84th percentile C_R between $T_{\tan}=5s-\infty$ with the initial damping model is between 8.1 and 8.5. However, when $R=8$ and $\beta=20\%$, the variation of the 84th percentile C_R between $T_{\tan}=5s-\infty$ with the tangent damping model is 37.0 and 19.4.

In general, these observations show that the influences of different hysteretic parameters on the 84th percentile C_R are similar to their influences on the median C_R .

CHAPTER 4:

REGRESSION ANALYSIS

4.1 Previous Proposals

It has been shown throughout Chapter 3 that the equal displacement assumption is not good enough to be used for self-centering SDOF systems. Therefore, this chapter aims to develop an equation to quantify the influence of the parameters of an self-centering SDOF system for design purposes.

The equal energy assumption and the equal displacement assumption are sometimes used for traditional elastoplastic systems in different period ranges (Filiatrault et al. 2013). The equal energy assumption has the form of $C_R = \frac{R^2 + 1}{2R}$ and hence is a constant for a give value of R . This is not consistent with the observation of Fig. 3.1 and Fig.3.11, which shows that C_R also depends on T_0 and β . On the other hand, it has been shown throughout Chapter 3 that the equal displacement assumption is generally unconservative for self-centering SDOF systems.

The only general equation available that has been proposed previously to estimate peak displacements of self-centering SDOF systems available was developed by Seo (2005) and the equation has been summarized in Chapter 1. It

can estimate the displacement demand generally within an accuracy of 20% for the initial damping model, but it is limited to $R = 1.5 - 8$.

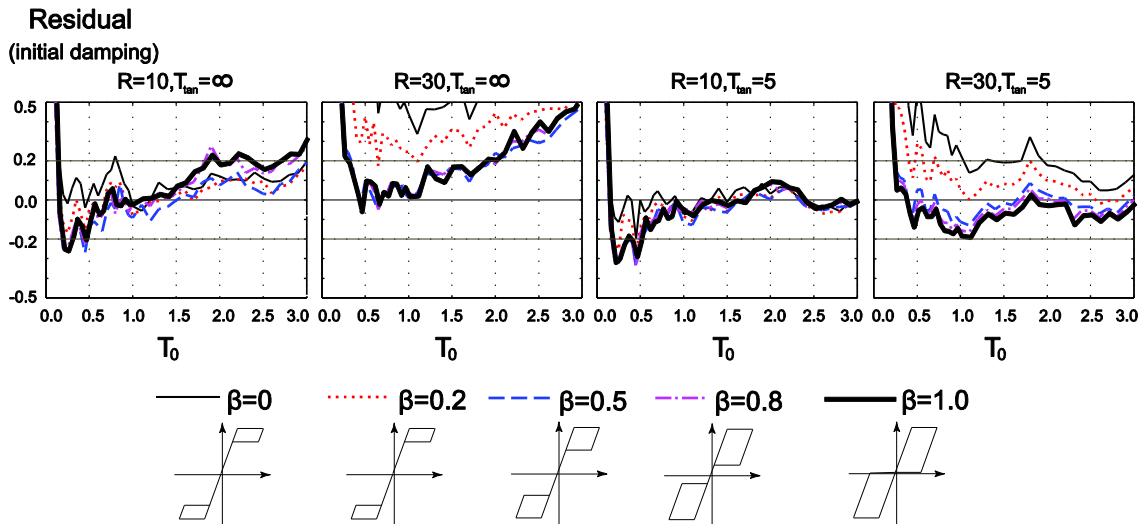


Figure 4.1 Residuals for Seo's Equation for Large R (based on Seo 2005)

To evaluate this equation for $R > 8$, the residual is defined as

$$Residual = \frac{C_{R,predicted} - C_{R,observed}}{C_{R,observed}} \quad (4-1)$$

By this definition, a positive residual means that the equation conservatively overestimates the displacement and a negative residual means that it unconservatively underestimates the displacement. Fig.4.1 shows that Seo's equation does not capture the results of this study for large R values. When R is slightly larger than the range what was used to develop Seo's equation ($R = 10$), that equation still works reasonably well, although it underestimates the displacement ratio by up to 30% around $T_0 = 0.2 - 0.5s$ and $\beta \geq 0.5$. The equation

also overestimates the displacement ratio by up to 30% when $T_0 \geq 1.5s$, $\beta > 0.5$, and $T_{\tan} = \infty$. When R becomes even larger ($R=30$) and $T_{\tan} = \infty$, significant overestimation is observed, which is more than 50% at short or long initial periods or with no energy dissipation. The equation is more accurate when $T_{\tan} = 5s$, but it still tends to overestimate the displacements when T_0 is very short or when there is little hysteretic energy dissipation.

4.2 Form of Regression Equation

The form of the proposed equation is based on the observation of trends from Chapter 3. First of all, the factor that has the biggest influence is T_0 . According to the observations of Fig. 3.1, Fig.3.11 and Fig.3.14 that the C_R decreases exponentially with increasing T_0 , the influence of T_0 can be captured by form of

$$\frac{c_2}{T_0^{c_1}} \times f(\beta, R, T_{\tan}) + c_3.$$

Based on Chapter 3, the second most important parameter is R . Fig.3.2 and Fig.3.12 showed that C_R increases with R but that the influence decreases as R becomes larger. Therefore, the form of $(R-c_3)^{c_4}$ with $c_4 < 1$ was selected. According to the definition of the force reduction factor, $R \geq 1$ and $R=1$ means that the system is elastic and therefore $C_R=1$. Therefore

$\frac{c_2}{T_0^{c_1}} \times (R-1)^{c_3} \times f(\beta, T_{\tan}) + 1$ is chosen for the regression analysis to ensure that whenever $R=1$, $C_R = 1$.

Thirdly, as for the influence of β , Fig.3.4 and Fig.3.13 show that the influence of β is smaller when β is closer to 1.0. Therefore, the influence of β is taken in

the form of $\frac{c_2}{T_0^{c_1}} \times (R-1)^{c_3} \times [c_4 + c_5(1-\beta)^{c_6}] \times f(T_{\tan}) + 1$.

Finally, T_{\tan} was shown to be the least important parameter as long as it is positive and not very short. If $T_{\tan} > 0$ is achieved, the shorter T_{\tan} is (i.e. the stiffer the system is in the nonlinear range), the smaller the displacement demand will be. Therefore, it is conservative to neglect the beneficial influence of increasing the nonlinear stiffness above $T_{\tan} = \infty$ in the regression. Doing this is likely to be reasonably accurate for practical values of T_{\tan} (about $T_{\tan} > 5s$), as will be verified subsequently.

Based on the discussions above, the following equation form is proposed:

$$C_R = (R-1)^{b_1} \frac{b_2 + b_3(1-\beta)^{b_4}}{T_0^{b_5}} + 1 \quad (4-3)$$

where b_1 , b_2 , b_3 , b_4 and b_5 are constants to be determined by regression.

Other forms of equation are also possible, including different polynomials, lognormal functions and exponential functions. However, Eq.(4-3) was judged to achieve a good balance between simplicity and accuracy for design purposes.

4.3 Calibration of Regression Equation

Only the results of $0.2s \leq T_0 \leq 3.0s$ are considered in the regression. This is because $\frac{c_1}{T_0^{c_2}} \rightarrow \infty$ as $T_0 \rightarrow 0$. The increase of C_R as $T_0 \rightarrow 0$ from the analyses is not as sharp as this form implies, and therefore the results at $T_0 < 0.2s$ dominated the regression when they were included. Also, as discussed before, self-centering systems may not be advisable for structures with very short initial periods because C_R tends to be very large. However, the regression that is developed for $T_0 \geq 0.2s$ will still be checked for $T_0 < 0.2s$.

Only $4 \leq R \leq 30$ are considered in the regression because the results with larger values of R may not be reliable, as discussed around Fig.3.3. On the other hand, a force reduction factor of $R = 2$ is not included because it is considered too small to take advantage of the benefits of a rocking or other self-centering system.

The results with $\beta \leq 10\%$ are also not considered in the regression because they tended to dominate the regression and because most design proposals for self-

centering systems recommend providing at least some energy dissipation (ACI T1.1-01, Eatherton et al. 2014, SCNZ 2015).

Based on the discussions above, only selected values listed in Table 2.1 (Section 2.1) are included in the regression and are summarized in Table 4.1.

Table 4.1 Parameters Considered in Regression Analysis

Parameter	Considered range
Initial period T_0	$0.2s \leq T_0 \leq 3.0s$
Force reduction factor R	$4 \leq R \leq 30$
Hysteretic energy dissipation parameter β	$20\% \leq \beta \leq 100\%$
Tangent period	$T_{\tan} = \infty$

The function of “fitlm” in MATLAB (MathWorks 2014a) is used to minimize the difference between $\frac{C_{R,predicted}}{C_{R,observed}}$ and 1. $C_{R,predicted}$ is the form of function that has been come up in Section 4.1. $C_{R,observed}$ is the results presented in Chapter 3. This function uses an iterative generalized least squares algorithm to fit the nonlinear regression model (MATLAB 2014a). The coefficients determined by regression are summarized In Table 4.2.

Table 4.2 Coefficient from Regression Analyses

			b_1	b_2	b_3	b_4	b_5	Root Mean Squared Error of $\frac{C_{R,predicted} - C_{R,observed}}{C_{R,observed}}$
Soil Sites	c_i	2%	0.774	0.071	0.088	1.290	1.641	10%
		5%	0.515	0.184	0.119	1.173	1.478	13%
		10%	0.341	0.297	0.122	1.081	1.344	7.4%
	c_i	5%	0.630	0.292	0.477	1.697	1.567	16%
Rock Sites	c_i	5%	0.469	0.052	0.047	1.251	1.708	8.4%

4.4 Evaluation of Regression

Fig.4.2 shows the residuals for 5% initial damping and tangent damping regression results, calculated according to Eq.4.1. For the regression equation developed for the initial damping model, the residuals are generally accurate to within 20% , and the equation is most accurate for intermediate R values ($8 \leq R \leq 15$). The equation tends to underestimate the displacement ratio when $T_0 \leq 0.3s$ and to overestimate when $T_0 \geq 2.0s$ and $R = 30$. The accuracy is similar for all values of β that were included in the regression ($0.2 \leq \beta \leq 1.0$). The regression equation developed for the tangent damping model tends to have slightly larger errors than the initial damping model, but is still generally accurate to within 20% for $\beta \geq 20\%$.

Values not considered in the regression (e.g. $\beta = 0$, $T_0 \leq 0.15s$) are also shown in Fig. 4.2. For $T_0 \leq 0.15s$, the regression equation underestimates the displacement

ratio by up to 70% for the initial damping model, and this underestimation is even more for tangent damping model (up to 90%). If the equation is used for $\beta = 0$ with the initial damping model, the residuals are only slightly larger than that for $\beta \geq 0.2$. However, the equation greatly overestimates the displacement ratio when $\beta = 0$ with the tangent damping model, especially at short periods. This overestimation is more significant for large R values, and it can be as large as five times the observed displacement ratio when $R = 30$.

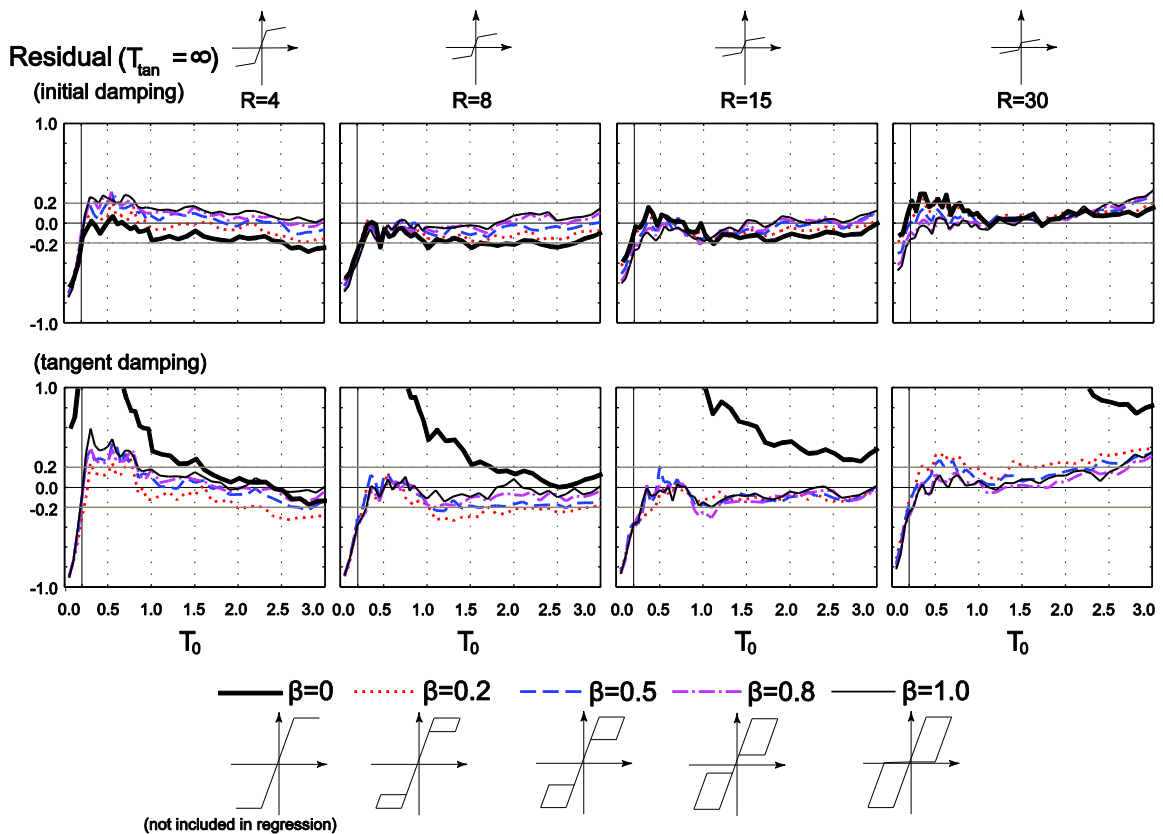


Figure 4.2 Relative Error between Predicted and Observed Displacement Demands (with $T_{\tan} = \infty$)

Fig.4.3 shows the validation of the same equation for $T_{tan} = 10s$ instead of $T_{tan} = \infty$. For the initial damping model, the equation is slightly more conservative compared to the results for $T_{tan} = \infty$ in Fig.4.2. For the tangent damping model, the tendency of overestimation is more significant when compared to that in Fig.4.2, especially for $\beta = 0.2$, but still within 20% in most cases.

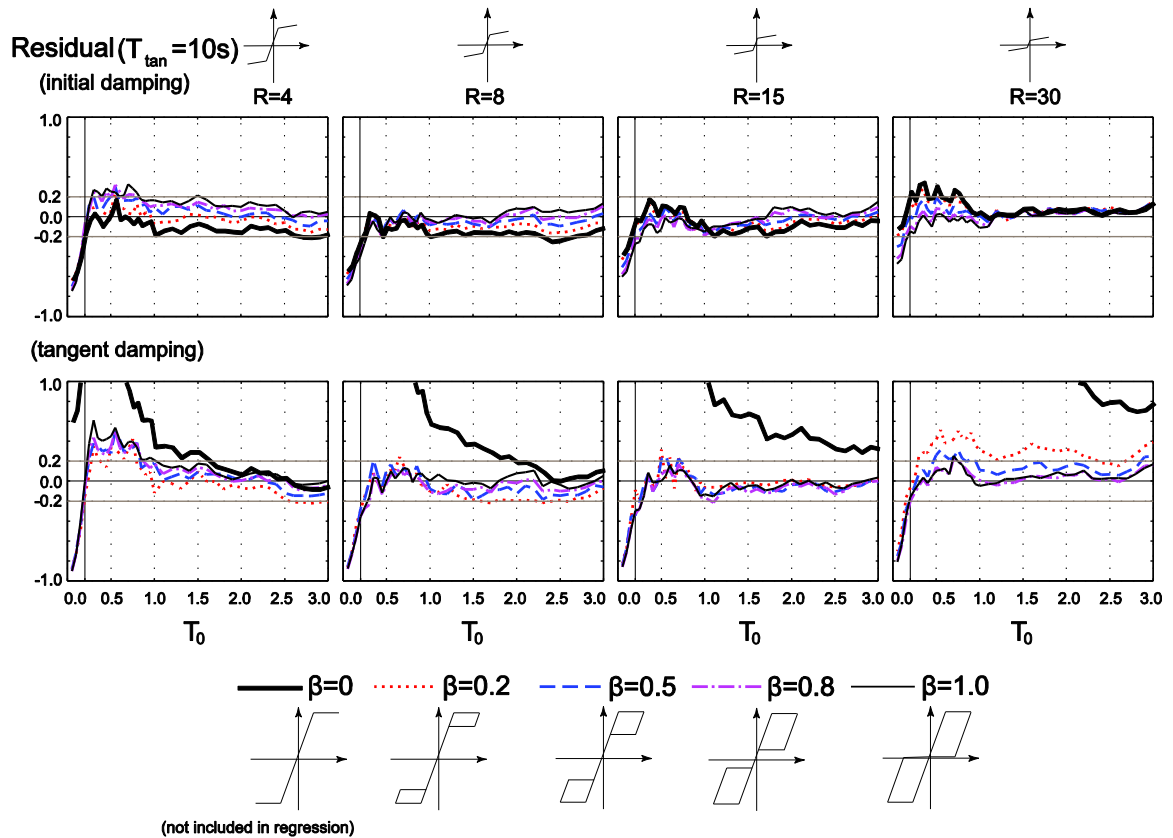


Figure 4.3 Relative Error between Predicted and Observed Displacement Demands with Tangent Period of 10s

CHAPTER 5:

CONCLUSIONS AND RECOMMENDATIONS

5.1 Conclusions

The first major contribution of this thesis was to present a parametric study on the seismic response of self-centering systems expressed in terms of displacement coefficient C_R , defined as the peak inelastic displacement of a self-centering system divided by the peak displacement of an elastic system with same initial period. Increasing the initial period generally decreases C_R . At short periods, C_R becomes very large, but the actual displacement may still be within acceptable limit (e.g. 2.5% of the height). Reducing the linear limit can double the peak displacement when the force reduction factor is small ($R \leq 8$), but the peak displacements become less sensitive to the linear limit when the force reduction factor is already greater than about $R = 10$. The effect of the linear limit is more pronounced at short initial periods. Increasing the hysteretic energy dissipation generally reduces the peak displacements by up to 50% when comparing the case of maximum self-centering hysteretic energy dissipation ($\beta = 1$) to that of no hysteretic energy dissipation ($\beta = 0$), but increasing β generally has diminishing returns. Also, the energy dissipation parameter affects systems with short periods ($T_0 \leq 0.5$ s) more than systems with long periods, and it influences systems with intermediate linear limits ($4 \leq R \leq 10$) more than systems with lower and higher

linear limits. If the nonlinear stiffness is positive but small ($5s \leq T_0 < \infty$), it has little influence. However, if it is negative due to $P-\Delta$ effects, the response can become unstable when the linear limit is low, the initial stiffness is small, or the nonlinear stiffness is much less than zero. Increasing hysteretic energy dissipation can only suppress nonlinear response before a critical negative stiffness that can cause collapse is reached; it generally cannot prevent the collapse caused by negative nonlinear stiffness. Based on this observation, it is not recommended to design structures to have a negative nonlinear stiffness if the linear limit is low or the initial stiffness is small.

When a different damping ratio is used with the initial damping model, the influences of different parameters are similar. However, when ground motions recorded on rock sites are used, C_R is systematically lower than the results using ground motions recorded on stiff soil sites.

In addition to the initial stiffness proportional damping model, a tangent stiffness proportional damping model was also considered. The general trends of variation of C_R with respect to different parameters were the same regardless of which damping model was used, but the tangent damping model led to a much larger displacement response compared to the displacement response when the initial stiffness proportional damping was used. Also, the effect of supplemental energy dissipation was more pronounced.

The second major contribution of this thesis was to quantify the effect of these parameters with a simplified equation. Neither the equal energy assumption nor the equal displacement assumption captures the median response of self-centering systems with acceptable accuracy. Therefore, an empirical equation was developed to estimate the median peak nonlinear displacement of a self-centering structure from its hysteretic properties as a multiplier of the elastic spectral displacement. The equation is simple enough to use for design and is also accurate to within 20% in most cases. Different coefficients were developed to account for different damping models in the regression equation.

More experimental data are needed to support recommendations for modelling damping in self-centering systems. In the absence of such recommendations, it is more conservative and therefore advisable to use the regression equation developed for the tangent damping model.

5.2 Recommendations for Future Work

This study is limited to ground motions recorded on rock and relatively stiff soil sites. The influence of different soil site conditions needs to be addressed.

The ground motion records used in this study are representative of the seismic hazard in California, and hence the results needs further scrutiny before using the results in other regions, including eastern North America.

Collapse was observed in some cases when the stiffness in the nonlinear range was negative while the initial stiffness and linear limit were both relatively low. Future research would be required to fully quantify the fragility of self-centering systems with a negative nonlinear stiffness, so as to develop detailed recommendations about the use of negative nonlinear stiffness in design.

The tangent damping model considered in this study leads to a significant larger displacement demands than the initial damping model. Future experimental tests are desired to examine which damping model is more realistic.

This study is focused on self-centering SDOF systems as a simplification of real multi-degree-of-freedom structures. Further work needed to apply the SDOF results of this study to real self-centering systems.

REFERENCES

- Abrahamson, N.A. and Silva, W.J. (1997). Empirical response spectral attenuation relations for shallow crustal earthquakes, *Seismological Research Letters*, 98: 94-127.
- ACI Innovation Task Group 1 and Collaborators, (2001) “Acceptance criteria for moment frames based on structural testing (T1.1-01) and Commentary (T1.1R-01)”, American Concrete Institute, Farmington Hills, Michigan, U.S.A..
- Ancheta, D.T., Darragh, B.R., Stewart, P.J., Seyhan, E., Silva, W.J., Chiou, S.J.B., Wooddell, E.K., Graves, W.R., Kottke, R.A., Boore, M.D., Kishida, T. and Donahue, L.J., (2013). PEER NGA-West2 Database”, *PEER Report*, Pacific Earthquake Engineering Research Center, Headquarters at the University of California, Berkeley, California, U.S.A..
- Baker, J.W., Lin, T., SHAHI, S.K. and Jayaram, N., (2011). “New ground motion selection procedures and selected motions for the PEER transportation research program”, *PEER Report*, Pacific Earthquake Engineering Research Center, College of Engineering, University of California, Berkeley, California, U.S.A..
- Boore, D.M., Joyner, W.B., and Fumal, T.E., (1997). Equations for estimating horizontal response spectra and peak acceleration from western North American earthquakes: a summary of recent work, *PEERSeismological Research Letters*, 68, 128-153.
- Charney, F., (2008) “Unintended consequences of modelling damping in structures”, *Journal of Structural Engineering*, 134(4), 581-592.
- Chopra, A.K., (2012), *Dynamics of structures: theory and application to earthquake engineering. 4th edition*, Upper Saddle River, N.J.: Prentice Hall.
- Christopoulos, C., Filiatrault, A. and Folz, B. (2002) “Seismic response of self-centering hysteretic SDOF systems”, *Earthquake Engineering and Structural Dynamics*, 31(5), 1131-1150.
- Christopoulos, C., Filiatrault, A., Uang, C-M, and Folz, B. (2002) “Posttensioned energy dissipating connections for moment-resisting steel frames”, *Journal of Structural Engineering*, 128(9), 1111-1120.
- Clifton, C., Bruneau, M., Macrae, G., Leon, R., and Fussell, A. (2011). “Steel structures damage from the Christchurch Earthquake series of 2010 and 2011.”, *Bulletin of the New Zealand Society for Earthquake Engineering*, 44(4), 298-318.
- Erochko, J., Christopoulos, C., Tremblay, R., and Kim, H.-J., (2013) “Shake table testing and numerical simulation of a self-centering energy dissipative

- braced frame”, *Earthquake Engineering and Structural Dynamics*, 42(11), 1617-1635.
- Eatherton, M., Ma, X., Krawinkler, H., Mar, D., Billington, S., Hajjar, J., and Deierlein, G. (2014) “Design concepts for controlled rocking of self-centering steel-braced frames”, *Journal of Structural Engineering*, 140(11), 10.1061/(ASCE)ST.1943-541X.0001047,04014082.
- FEMA (Federal Emergency Management Agency). (2009). Effects of strength and stiffness degradation on seismic response. *Report FEMA 440A*. Washington DC: Federal Emergency Management Agency.
- Filiatrault, A., Tremblay, R., Christopoulos, C., Folz, B., and Pettinga, D., (2013), *Elements of Earthquake Engineering and Structural Dynamics, 3rd edition*, Montreal, Quebec: Presses Internationales Polytechnique.
- Iwata, Y., Sugimoto, H., and Kuwamura, H.(2005). “Reparability limit of steel structural buildings based on the actual data of the Hyogoken-Nanbu Earthquake”, *Journal of Structural and Construction Engineering: Transactions of AIJ*, 588, 165-172.
- Kam, W., Pampanin, S., Dhakal, R., Gavin, H., and Roeder, C. (2010). “Seismic performance of reinforced concrete buildings in the September 2010 Darfield (Cantebury) Earthquake”, *Bulletin of the New Zealand Society for Earthquake Engineering*, 43(4), 340-350.
- Kurama, Y. (2000) “Seismic design of unbonded post-tensioned precast concrete walls with supplemental viscous damping”, *ACI Structural Journal*, 97(4), 648-658.
- Leger, P. and Dussault, S., (1992). “Seismic energy dissipation in MDOF structures”, *Journal of Structural Engineering*, 118(5), 1251-1269.
- MathWorks, (2014a), MATLAB 2014a student version, Natick, Massachusetts, U.S.A..
- Ma, X., Krawinkler, H., and Deierlein, G.G. (2011). “Seismic design and behavior of self-centering braced frame with controlled rocking and energy dissipating fuses.” *Rep. No. 174*, the John A. Blume Earthquake Engineering Center, Stanford University, Stanford, California, U.S.A..
- McCormick, J., Abrano, H., Ikenaga, M., and Nakashima, M. (2008). “Permissible residual deformation levels for building structures considering both safety and human elements”, *The 14th World Conference on Earthquake Engineering, Beijing, China*, Paper ID 05-06-0071.
- Miranda, E., (2000), “Inelastic displacement ratios for structures on firm sites”, *Journal of Structural Engineering*, 126(10) 1150-1159.
- Newmark, N.M., and Hall, W.J., (1982). *Earthquake spectra and design*, Earthquake Engineering Research Institute, Berkeley, California, U.S.A..

- NRCC (National Research Council Canada), (2010) “*National building code of Canada 13th edition*”, Ottawa, Ontario, Canada.
- Park, R., and Paulay, T.(1975). *Reinforced concrete structures*, John Wiley & Sons, Inc., New York.
- PEER 2011. <http://peer.berkeley.edu/transportation/projects/ground-motion-studies-for-transportation-systems/> Pacific Earthquake Engineering Center, Berkeley, California, U.S.A..
- Priestley, M.J.N., and Tao, J-R. (1993) “Seismic Response of precast prestressed concrete frames with partially debonded tendons”, *PCI Journal*, 38(1), 58-69.
- Priestley, M.J.N. and Grant, D.N., (2005). “Viscous damping in seismic design and analysis”, *Journal of Earthquake Engineering*, 9(s2), 229-255.
- Restrepo, J., and Rahman, A. (2007) “Seismic performance of self-centering structural walls incorporating energy dissipators”, *Journal of Structural Engineering*, 133(1), 1560-1570.
- Roh, H., and Reinhorn, A. (2010). “Modeling and seismic response of structures with concrete rocking columns and viscous dampers”, *Engineering Structures*, 32(8), 2096-2107.
- Steel Construction New Zealand (SCNZ), (2015). *Design guide for controlled rocking steel braced frames*. Draft dated 22 April 2015, publication pending by SCNZ, Manukau City, NZ.
- Seo, C-Y., and Sause, R., (2005) “Ductility demands on self-centering systems under earthquake loading”, *ACI Structural Journal*, 102(2), 275-285.
- Seo, C-Y., (2005) “Influence of ground motion characteristics and structural parameters on seismic responses of SDOF systems”, PhD Dissertation, Lehigh University, Bethlehem, Pennsylvania, U.S.A..
- Shome, N. and Cornell, C.A., (1999) Probabilistic seismic demand analysis of nonlinear structures, *Report No.RMS-35, Reliability of Marine Structures*, Department of Civil Engineering, Stanford University, Stanford, California, U.S.A..
- The New Zealand Herald, “Govt reveal post-quake rebuild costs for Greater Christchurch”, Internet reference, URL: http://www.nzherald.co.nz/nz/news/article.cfm?c_id=1&objectid=10852452 , published December, 2012, accessed March, 2015.
- Wiebe, L. and Christopoulos, C., (2009) “Mitigation of higher mode effects in base-rocking system by using multiple rocking joints”, *Journal of Earthquake Engineering*, 13(S1) 83-108.
- Wiebe, L., Christopoulos, C., Tremblay, R. and Leclerc, M., (2013) “Mechanisms to limit higher mode effects in a controlled rocking steel frame. 1: concept,

modelling, and low-amplitude shake table test”, *Earthquake Engineering and Structural Dynamics*, 42(7), 1053-1068.

Wiebe, L., and Christopoulos, C., (2014). “Performance-based seismic design of controlled rocking steel braced frames. I: methodological framework and design of base rocking joint”, *Journal of Structural Engineering*, available online ahead of print, DOI: 10.1061/(ASCE)ST. 1943-541X.0001202.

APPENDIX A:

VALIDATION OF NUMERICAL SOLUTION TECHNIQUE

A.1 Validation of Numerical Solution Technique for Initial Damping Model

Before going into detailed study, the numerical solution technique needs to be checked. A previous published journal paper was used for this check (Christopoulos et al. 2002).

Christopoulos et al. (2002) used a set of 20 ground motion records and calculated the mean displacement ductility for self-centering SDOF systems with the initial stiffness proportional damping model. A figure summarizing the results from the journal paper is shown as Fig.A.1.

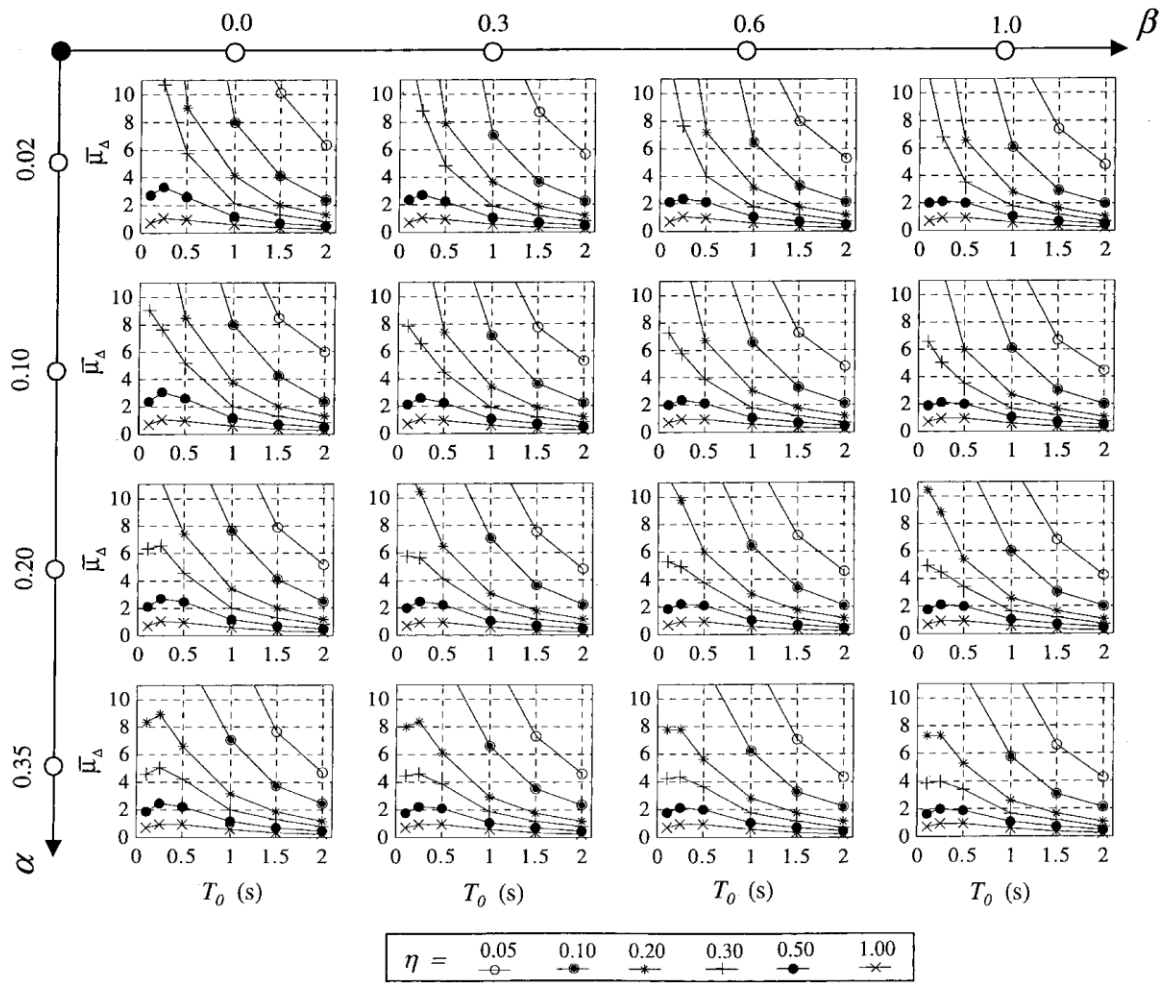


Figure A.1 Mean displacement ductility for flag-shaped hysteretic systems (taken from Christopoulos et al. 2002)

The definitions of α and β are the same as described in Chapter 2.

The strength ratio is defined as

$$\eta = \frac{C_v I}{RT_0} \quad (\text{Eq. A-1})$$

where $C_v = 0.64$ is related to code provisions on seismic zone and site conditions;

$I = 1.0$ is the importance factor;

$4.5 \leq R \leq 8.5$ is the force reduction factor;

T_0 is the initial period.

The displacement ductility is defined as:

$$\bar{\mu}_{\Delta} = \frac{\Delta_{nonlinear}}{(\Delta_{elastic} / R)} \quad (\text{Eq. A-1})$$

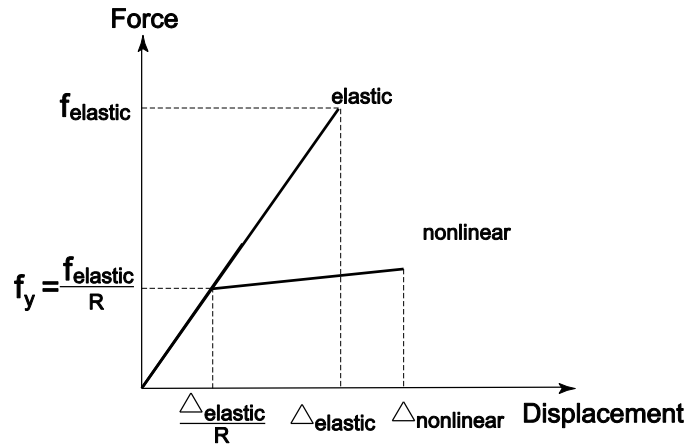


Figure A.2 Definition of displacement ductility

Using the numerical solution technique described in Chapter 2 and the same ground motion records, the results from the author's code is summarized in Table A.1, Table A.2, Table A.3 and Table A.4. Table A.1 corresponds to the figures in the first row of Fig.A.1, Table A.2 corresponds to the figures in the second row of Fig.A.2 and so on.

Table A.1 Displacement ductility with $\alpha = 0.02$

β	η	$\bar{\mu}_\Delta$					
0	0.05	292.706	155.553	48.263	16.680	10.012	6.289
	0.1	132.537	68.118	25.165	7.959	4.091	2.359
	0.2	43.001	29.398	9.045	4.078	2.024	1.236
	0.3	15.138	12.109	5.721	2.058	1.321	0.806
	0.5	2.700	3.364	2.528	1.152	0.719	0.457
	1.0	0.756	1.108	0.962	0.533	0.358	0.227
0.3	0.05	286.239	149.937	45.256	15.555	8.658	5.608
	0.1	127.695	65.219	22.966	7.028	3.617	2.165
	0.2	39.455	25.283	7.857	3.623	1.874	1.175
	0.3	12.976	10.564	4.793	1.872	1.217	0.763
	0.5	2.315	2.895	2.229	1.085	0.716	0.455
	1.0	0.753	1.081	0.956	0.533	0.358	0.227
0.6	0.05	280.097	143.953	42.955	14.483	7.996	5.256
	0.1	122.660	62.178	20.664	6.396	3.222	2.065
	0.2	36.714	22.989	7.104	3.212	1.735	1.130
	0.3	11.631	8.742	4.030	1.786	1.182	0.749
	0.5	2.121	2.570	2.106	1.041	0.714	0.453
	1.0	0.751	1.069	0.952	0.533	0.358	0.227
1.0	0.05	271.493	137.277	40.064	13.315	7.367	4.761
	0.1	115.713	57.895	18.076	6.066	2.950	1.950
	0.2	35.855	19.592	6.491	2.795	1.607	1.080
	0.3	11.018	7.805	3.542	1.699	1.150	0.745
	0.5	1.963	2.329	1.973	1.012	0.714	0.450
	1.0	0.748	1.058	0.947	0.533	0.358	0.227

Table A.2 Displacement ductility with $\alpha = 0.10$

β	η	$\bar{\mu}_\Delta$					
0	0.05	115.436	99.820	41.306	15.489	8.381	5.956
	0.1	51.781	45.611	19.358	7.916	4.190	2.395
	0.2	20.187	16.163	8.466	3.741	2.018	1.235
	0.3	9.095	8.868	5.137	2.005	1.292	0.801
	0.5	2.328	3.045	2.518	1.147	0.719	0.457
	1.0	0.755	1.098	0.962	0.533	0.358	0.227
0.3	0.05	114.322	97.161	39.565	14.567	7.771	5.274
	0.1	50.114	43.685	17.747	7.146	3.678	2.222
	0.2	18.591	14.559	7.399	3.369	1.838	1.166
	0.3	7.840	7.226	4.400	1.855	1.212	0.761
	0.5	2.104	2.819	2.241	1.085	0.716	0.455
	1.0	0.753	1.077	0.957	0.533	0.358	0.227
0.6	0.05	113.288	94.801	38.074	13.705	7.258	4.806
	0.1	48.664	41.577	16.608	6.597	3.333	2.093
	0.2	17.154	13.491	6.679	3.038	1.732	1.128
	0.3	7.160	6.326	3.808	1.774	1.174	0.747
	0.5	1.991	2.509	2.101	1.040	0.714	0.453
	1.0	0.751	1.065	0.952	0.533	0.358	0.227
1.0	0.05	111.713	91.456	35.759	13.026	6.659	4.445
	0.1	47.199	39.223	15.052	6.037	3.006	1.984
	0.2	16.256	12.562	5.933	2.703	1.632	1.084
	0.3	6.521	5.491	3.452	1.692	1.146	0.744
	0.5	1.863	2.235	1.960	1.010	0.714	0.450
	1.0	0.749	1.055	0.948	0.533	0.358	0.227

Table A.3 Displacement ductility with $\alpha = 0.20$

β	η	$\bar{\mu}_{\Delta}$					
0	0.05	71.692	64.846	33.976	14.649	7.787	5.144
	0.1	32.306	30.134	15.368	7.657	4.093	2.409
	0.2	12.814	12.308	7.382	3.357	1.990	1.224
	0.3	6.338	6.793	4.533	1.998	1.271	0.789
	0.5	2.119	2.982	2.448	1.144	0.718	0.456
	1.0	0.755	1.086	0.962	0.533	0.358	0.227
0.3	0.05	70.410	63.329	32.957	13.795	7.466	4.824
	0.1	31.201	28.883	14.439	6.989	3.575	2.267
	0.2	12.041	11.183	6.481	3.099	1.802	1.164
	0.3	5.669	5.926	4.060	1.846	1.208	0.761
	0.5	2.001	2.639	2.220	1.084	0.716	0.455
	1.0	0.753	1.071	0.957	0.533	0.358	0.227
0.6	0.05	69.161	62.053	32.013	13.070	7.141	4.529
	0.1	30.337	27.755	13.691	6.446	3.338	2.153
	0.2	11.259	10.432	5.910	2.878	1.719	1.125
	0.3	5.273	5.339	3.715	1.766	1.165	0.745
	0.5	1.894	2.337	2.083	1.043	0.714	0.453
	1.0	0.752	1.062	0.953	0.533	0.358	0.227
1.0	0.05	67.665	60.391	30.851	12.270	6.760	4.264
	0.1	29.299	26.340	12.870	5.905	3.064	2.036
	0.2	10.387	9.739	5.419	2.625	1.642	1.087
	0.3	4.824	4.793	3.425	1.689	1.142	0.742
	0.5	1.773	2.165	1.944	1.010	0.713	0.451
	1.0	0.749	1.052	0.949	0.533	0.358	0.227

Table A.4 Displacement ductility with $\alpha = 0.35$

β	η	$\bar{\mu}_\Delta$					
0	0.05	43.613	41.683	27.549	14.196	7.643	4.716
	0.1	19.941	20.192	13.478	6.995	3.773	2.447
	0.2	8.298	9.076	6.554	3.200	1.912	1.222
	0.3	4.609	5.336	4.249	1.953	1.248	0.783
	0.5	1.866	2.561	2.281	1.131	0.718	0.456
	1.0	0.754	1.076	0.961	0.533	0.358	0.227
0.3	0.05	42.988	41.034	27.085	13.604	7.309	4.539
	0.1	19.507	19.365	12.885	6.579	3.503	2.298
	0.2	7.927	8.373	6.048	2.947	1.796	1.165
	0.3	4.395	4.855	3.909	1.840	1.201	0.762
	0.5	1.808	2.387	2.125	1.082	0.716	0.455
	1.0	0.753	1.064	0.957	0.533	0.358	0.227
0.6	0.05	42.424	40.428	26.550	13.078	7.002	4.346
	0.1	19.011	18.697	12.367	6.187	3.291	2.202
	0.2	7.655	7.820	5.638	2.778	1.714	1.121
	0.3	4.194	4.487	3.658	1.759	1.164	0.746
	0.5	1.755	2.249	2.023	1.048	0.715	0.453
	1.0	0.752	1.057	0.954	0.533	0.358	0.227
1.0	0.05	41.859	39.818	25.723	12.370	6.597	4.206
	0.1	18.512	18.078	11.771	5.731	3.069	2.108
	0.2	7.264	7.291	5.256	2.612	1.636	1.089
	0.3	3.871	4.106	3.384	1.688	1.137	0.739
	0.5	1.684	2.108	1.923	1.014	0.713	0.452
	1.0	0.750	1.048	0.950	0.533	0.358	0.227

Checking the results in the tables with the figure, most data matches the data points in Fig.A.1 well. But a few points seem to be problematic, which are red-bolded. The inconsistency of these few data is noticeable but not very large. These unmatched points were checked with Dr. Lydell Wiebe, who has also

published research on self-centering SDOF systems (Wiebe and Christopoulos 2014). His calculations confirmed the results that are calculated in this thesis (within 0.2% accuracy). Based on this, the discrepancies in 8 out of 440 (shown in Fig. A.1) values were considered most likely to be due to a production error in the published paper, rather than a calculation error. Thus, these results were considered to validate the numerical solution program developed by the author.

A.2 Validation of Numerical Solution Technique for Tangent Damping Model

The code developed for the tangent damping model by the author is checked with the code developed by Dr. Lydell Wiebe, who has unpublished results regarding damping. The checks are summarized in Table A.5, Table A.6 and Table A.7 as follows. These analyses are based on the El-Centro ground motion record used in Chopra (2012). The time step is $0.001s$ using Newmark's scheme with constant average acceleration. The damping ratio $\zeta = 5\%$, assumed mass is unity (i.e. $m = 1$) and the gravity constant is $g = 9.81m/s^2$.

Notations for variables the used in these tables are:

- D_{wiebe} : displacement calculated from Wiebe's code;
 D_{zhang} : displacement calculated from the author's code;

$$Error = \frac{D_{zhang} - D_{wiebe}}{D_{wiebe}} \times 100\% : \text{relative difference between two the results.}$$

Table A.5 Summary of results checking with $T_0 = 0.2s$ and $R = 2$

Hysteretic Parameters		D_{zhang}	D_{wiebe}	$Error$
T_{tan} (s)	β			
∞	0%	0.008176	0.008185	0.1%
	50%	0.007640	0.007648	0.1%
	100%	0.007840	0.007850	0.1%
10	0%	0.008167	0.008176	0.1%
	50%	0.007634	0.007642	0.1%
	100%	0.007832	0.007842	0.1%
-20	0%	0.008176	0.008185	0.1%
	50%	0.007640	0.007648	0.1%
	100%	0.007840	0.007851	0.1%

Table A.6 Summary of results check with $T_0 = 1.0s$ and $R = 2$

Hysteretic Parameters		D_{zhang}	D_{wiebe}	Error
T_{tan} (s)	β			
∞	0%	0.1061	0.1061	0%
	50%	0.0879	0.0880	0.1%
	100%	0.0806	0.0806	0%
10	0%	0.1062	0.1062	0%
	50%	0.0876	0.0876	0%
	100%	0.0803	0.0804	0.1%
-20	0%	0.1059	0.1059	0%
	50%	0.0880	0.0880	0%
	100%	0.0806	0.0806	0%

Table A.7 Summary of results check with $T_0 = 2.0s$ and $R = 2$

Hysteretic Parameters		D_{zhang}	D_{wiebe}	Error
T_{tan} (s)	β			
∞	0%	0.2882	0.2879	0.1%
	50%	0.2066	0.2067	0.1%
	100%	0.1770	0.1769	0.1%
10	0%	0.2532	0.2533	0.1%
	50%	0.1926	0.1927	0.1%
	100%	0.1774	0.1774	0%
-20	0%	0.2759	0.2757	0.1%
	50%	0.2085	0.2086	0.1%
	100%	0.1756	0.1756	0%

The author's code for the tangent damping model can get results within 0.2% difference compared to the other. This slight difference may come from different programming details, such as the convergence criteria but is negligible. Therefore, these results were considered to validate the numerical solution program developed by the author.

APPENDIX B:

REGRESSION FOR MEAN VALUE

The mean values of C_R have similar trend with respect to different hysteretic parameters. Another regression analysis are carried out considering the mean C_R . Same range of parameters are considered (i.e. $T_0 = 0.05s - 3.0$, $4 \leq R \leq 30$, $0.2 \leq \beta \leq 1.0$ and $T_{\tan} = \infty$). Results are summarized in Table B.1.

Table B.1 Coefficients from regression analyses (Mean)

			b_1	b_2	b_3	b_4	b_5	Root Mean Squared Error of $\frac{C_{R,predicted} - C_{R,observed}}{C_{R,observed}}$
Soil Sites	c_i	5%	0.369	0.475	0.252	1.119	1.362	9.7%
		2%	0.496	0.324	0.299	1.254	1.490	12%
		10%	0.281	0.539	0.180	1.044	1.276	8.0%
	c_t	5%	0.413	0.929	1.246	1.489	1.628	18%
Rock Sites	c_i	5%	0.364	0.275	0.177	1.121	0.949	12%